POLITECNICO DI MILANO

School of Industrial and Information Engineering

Master of science in
Engineering Physics

Ultrafast pump-probe spectroscopy in the Ultra violet wavelength region

Supervisor: Prof. Giulio CERULLO

Co-Supervisor: Dr. Rocio BORREGO VARILLAS

Candidate:

Joel HAZAN Matr. 859270

Accademic Year 2017 - 2018

Alla mia famiglia con affetto e riconoscenza

Abstract

This thesis is focused on the development of a pump-probe spectroscopy setup in the ultraviolet, in order to study the dynamical response of important biomolecules. Pump-probe spectroscopy is a widely used ultrafast spectroscopic technique which provides valuable information on the nature and dynamics of photogenerated species in solids and molecules. By correlating the information content of the differential transmission signal for different probing wavelengths, pump-probe allows to measure spectral diffusion, couplings and energy transfers between energy levels. It has been successfully implemented in the infra-red and visible ranges. In the ultraviolet range, where most biomolecules absorb, it is expected to provide important information about the ultrafast dynamics and structural conformations of molecules such as DNA and proteins. The extension of pump-probe to the ultraviolet range although is not straightforward, because the technical difficulties become more challenging in this wavelength range. UV pulses are more energetic and could induce higher dispersion losses and higher order non linear effects. In the first chapter will be discussed the propagation of ultra-short pulses in a dispersive medium, and several non-linear optical generation processes that will be exploited in the setup. In the second chapter pump-probe is briefly explained, detailing the efforts done up to now to extend the technique to the ultraviolet range. The hyperspectral broadband pump probe experimental configuration is also presented, referring to all the non-linear processes presented in the previous chapter. After these introductory chapters, the employed setup is described, which is based on the pump-probe technique using excitation with tunable ultra short pump pulses in the UV. This allows us to obtain a set of transient absorption maps resolved in time, as a function of the detection frequencies, which contains information regarding both the absorption bands and the lifetimes of the energetic levels of the sample. The pump pulses are tunable in the 270 - 300 nm ultraviolet range, allowing us to excite electronic transitions in the test samples (Tryptophan, Azurin), while the probe can be chosen between a visible or ultraviolet white light continuum, covering the whole 300 - 700 nm range. In the fourth chapter we show results of measurements made to test the setup performance. Time-resolved pump-probe measurements are performed on Tryptophan and are accurately matched with the available experimental results. Lastly, starting from the analysis of a single aminoacid (tryptophan), we follow this with the measurement of a tryptophan-based metallo-protein (Azurin). By employing pump-probe measurement the aim is to investigate the differences between the Tryptophan alone dissolved in water as aminoacid and the mechanisms which appear when it is incorporated in more complex systems, such as the presence of a ligand to metal charge transfer (LMCT) absorption band in the Azurin spectrum of absorption.

Sommario

Questa tesi é incentrata sullo sviluppo della spettroscopia pump probe nell'ultravioletto, al fine di studiare la struttura di importanti biomolecole. La spettroscopia pump probe una tecnica spettroscopica ultraveloce, risolta in tempo e ampiamente utilizzata, che fornisce preziose informazioni sulla natura e la dinamica dei solidi e delle molecole, dopo che hanno subito uneccitazione fotonica. Correlando il contenuto informativo del segnale di trasmissione differenziale per diverse lunghezze d'onda di sondaggio, questa tecnica spettroscopica consente di misurare la diffusione spettrale, gli accoppiamenti e i trasferimenti di energia tra i vari stati energetici presenti nel sistema. É stato implementato con successo nelle regioni di frequenza infrarossa e visibile. Nella regione spettrale dellultravioletto, dove la maggior parte delle biomolecole assorbono energia, si prevede che forniscano informazioni importanti su dinamica ultraveloce e conformazioni strutturali di molecole complesse come il DNA e le proteine. L'estensione della spettroscopia pump probe allultravioletto non é semplice, poich le difficolt tecniche ne rendono pi impegnative le realizzazioni sperimentali. Impulsi ultravioletti infatti presentano alte energie e possono causare ingenti dispersioni e perdite. Nel primo capitolo verr discussa la propagazione degli impulsi ultra-corti in un mezzo dispersivo e diversi processi di generazione ottica non lineare che saranno sfruttati in seguito nella configurazione sperimentale. Nel secondo capitolo la tecnica pump probe é brevemente spiegata, ponendo maggiore attenzione su una configuratione spettroscopica a banda larga, dove limpulso di probe bianco, quindi possiede svariate frequenze. Dopo questi capitoli introduttivi, viene descritta la configurazione impiegata, che é basata sulla tecnica pump-probe mediante eccitazione sintonizzabile di impulsi ultrabrevi nell'UV. Questo ci consente di ottenere una serie di mappe di assorbimento risolte in tempo, in funzione delle frequenze di test (probe), che contengono informazioni riguardanti sia le bande di assorbimento che i tempi di vita dei livelli energetici del campione. Gli impulsi della pompa sono sintonizzabili nel regime dei raggi ultravioletti tra 260-300 nm , il che consente di eccitare transizioni elettroniche nei Campioni da studiare (Triptofano, Azurrina), mentre la sonda pu essere scelta tra un continuum a luce bianca visibile o ultravioletta, coprendo l'intero spettro tra 300 - 700 nm. Nel quarto capitolo mostriamo i risultati delle misurazioni effettuate per testare la configurazione e le relative prestazioni. Le misurazioni pump probe risolte in tempo sono eseguite su Triptofano e sono accuratamente abbinate ai risultati sperimentali disponibili. Infine, a partire dall'analisi di un singolo amminoacido (triptofano), seguiamo ci con la misura di una metalloproteina a base di triptofano (Azurrina). Utilizzando la misurazione pump probe, lo scopo é quello di indagare le differenze tra il triptofano da solo disciolto in acqua come amminoacido

e i meccanismi che compaiono quando esso é incorporato in sistemi pi complessi. Esempio di ció é la comparsa di una banda di assorbimento nello spettro dell'azzurrina, indicatrice di un trasferimento elettronico tra metallo e molecola organica(LMCT).

Contents

Introduction

One of the cornerstones of structural biology is the link between the protein sequence and its structure and function. Proteins are large biomolecules consisting of ensemble of long aminoacids chains (called poly-peptides). Aminoacids position and structure in the protein is strictly contained in the Dna genetic sequences. When they absorb light, aminoacids perform ultra fast processes such as photo-protection effect [1].
It's possible to track this effects performing ultra fast pump probe spectroscopy. Pump-probe spectroscopy is an advanced third-order non linear spectroscopic technique allowing us to fully recover the non linear polarization emitted by a sample. Through the recent development of Optical parametric amplification [2], which permits to obtain tunable ultra short pulses, this technique has been successfully implemented in the infra-red and visible ranges, targeting molecular aggregates [3], eye proteins [4] and graphene and low dimensional materials [5]. Many studies reveal that if pump probe spectroscopy is implemented in the UV range it is possible to appreciate signals deriving from many biomolecules. Moreover some aminoacids contain an aromatic benzenic ring residue; therefore they absorb in the 250-300 nm range. They are tryptophan, tyrosine and phenylalanine, but our discussion will focus on the Tryptophan analysis, because it is the most absorbing in the ultraviolet frequency range between those three. Tryptophan is called an essential aminoacid because it can not be produced by our body but it is assumed from our diet[6]. Since they rarely occur in proteins, interactions between aromatic residues would give characteristic signatures in an eventual transient spectra or dynamic. Moreover they can strongly link to other materials, exploiting very interesting effects. [7] Aggregating in proteins aminoacids create more complex systems and new kind of effects enter in play. Metallo-proteins are one of the most evident cases in which is present a strong link and an energy transfer between Tryptophan radicals and metal atoms[7].
This thesis is focused on the development of a pump probe spectroscopy setup in the ultraviolet frequency region, overcoming technical difficulties associated to the ultraviolet range. The final intent is to study the described interactions, starting from single aromatic aminoacids up to more complex aggregates such as proteins. Since we want to investigate molecular dynamics which appears in a very fast time ($\approx 100fs$), we need very high resolution in order to track this[8]. To implement this is needed to find a way to obtain ultra fast pulses in the ultraviolet as excitation beam in order to get high resolution system for the impulse response function of the experimental apparatus. This force us to have broadband pump having bandwidth around $50nm$, from 260 up to 310 nm. Otherwise when ultra-short pulses are not required, we can achieve the desired excitation frequency resolution by using narrowband pump pulses, in order to investigate slower effects, with less difference (ΔE) in the excitation energy.

Chapter 1

Nonlinear optical Processes

This chapter presents an explanation of the processes employed in the setup, starting from the linear propagation of an optical pulse and then introducing non linear phenomena, such as second harmonic generation, white light generation and optical parametric amplification.

1.1 Pulse Propagation

1.1.1 Linear Processes

To understand pulse propagation, one can start from the Maxwell equations:

$$\begin{cases} \nabla \cdot \mathbf{D} = \rho \\ \nabla \times \mathbf{E} = -\dfrac{\delta \mathbf{B}}{\delta t} \\ \nabla \cdot \mathbf{B} = 0 \\ \nabla \times \mathbf{H} = \mathbf{J} + \dfrac{\partial \mathbf{D}}{\partial t} \end{cases} \tag{1.1}$$

Where

$$\begin{cases} \mathbf{D} = \epsilon_0 \mathbf{E} + \mathbf{P} \\ \mathbf{B} = \mu_0 \mathbf{H} + \mathbf{M} \end{cases} \tag{1.2}$$

In addition to that, we are considering media with negligible magnetization ($\mathbf{M} \approx 0$), in absence of free charges ($\rho = 0$) and no current ($\mathbf{J} = 0$), a linearly polarized pulse propagating along the z direction, and no variation along the transversal direction (plane wave approximation). According to that the electric field could be expressed as

$$E(z,t) = \mathrm{A(z,t)e}^{\imath(\omega_0 t - k_0 z)} \tag{1.3}$$

where ω_0 is the carrier frequency, k_0 is the wave vector of the pulse and $\mathrm{A(z,t)}$ is the complex field amplitude. It is also possible then to derive the following equation

$$\frac{\partial^2 \mathrm{E}}{\partial \mathrm{z}^2} - \frac{1}{c^2}\frac{\partial^2 \mathrm{E}}{\partial t^2} = \mu_0 \frac{\partial^2 \mathrm{P}}{\partial t^2} \tag{1.4}$$

Equation (1.4) is a wave equation where the right hand polarization term can be seen as the source term. Similarly to the electric field, the polarization P in a linear medium,can be written as

$$\mathrm{P(z,t)} = \mathrm{p(z,t)e}^{\imath(\omega_0 t - k_p z)} \tag{1.5}$$

and can be decomposed into a sum of linear and non linear component

$$\mathrm{P(z,t)} = \mathrm{P_L} + \mathrm{P_{NL}} \tag{1.6}$$

where each term can be described by its own amplitude $p_L(z,t)$ and $p_{NL}(z,t)$,and $k_p \neq k_0$. For the moment we will neglect non-linear terms, then by Taylor expansion of the wavevector k around the frequency $\omega - \omega_0$.

$$\mathrm{k}(\omega) = k_0 + \frac{\partial k}{\partial \omega}|_{\omega=\omega_0}(\omega - \omega_0) + \frac{1}{2}\frac{\partial^2 \mathrm{k}}{\partial \omega^2}|_{\omega=\omega_0}(\omega - \omega_0)^2 \tag{1.7}$$

defining the velocity of the envelope ($\mathrm{v_g}$,called group velocity and the group velocity dispersion (GVD).

$$\begin{aligned} \frac{1}{v_g} &= \frac{\partial k}{\partial \omega}|_{\omega=\omega_0} \\ GVD &= \frac{\partial^2 k}{\partial \omega^2}|_{\omega 0} \end{aligned} \tag{1.8}$$

We have to assume a last approximation in order to simplify computations: the Slowly Varying Envelope Approximation (SVEA), which consists in neglecting envelope variations over propagation lengths of the order of a wavelength. During propagation in a non-dispersive medium (refractive index independent from frequency $n(\omega) = const$),pulses acquire a linear phase, but their shape remains unchanged. The delay of a pulse is the group delay $\tau_g = \frac{L}{v_g}$. In a dispersive medium, propagation introduces higher order terms in the acquired phase. It is useful to define the Group Delay Dispersion (GDD, or D_2) which accounts for the accumulated second order dispersion in a material of length L:

$$GDD = \frac{\partial^2 k}{\partial \omega^2}|_{\omega=\omega_0} L \tag{1.9}$$

The effect on the propagation of a dispersive medium could be analytically calculated for a Gaussian pulse. Its duration increases according to the law

$$\tau = \tau_p \sqrt{1 + \left(\frac{L}{L_D}\right)^2}. \tag{1.10}$$

where $L_D = \frac{\tau_p^2}{k_0''}$ is the dispersion length. When $L < L_D$ (short propagation distances) the pulse width doesn't change significantly, while for very long L the broadening is almost linear with respect to propagation distance. Taking that into account, the ultrashort pulse can be written as

$$E(z,\tau) = A(z,\tau)e^{\imath(\omega_0\tau - \phi(\tau) - k_0 z)} \tag{1.11}$$

the istantaneous frequency is:

$$\omega_i = \omega_0 + \frac{\partial\phi}{\partial\tau} = \omega_0 + \frac{D_2\tau}{(\tau_p^4 + D_2^2)} \tag{1.12}$$

Thus, frequency is not constant but shows a linear variation or chirp, depending on D_2. If $D_2 > 0$ we have a positive chirp (frequency increases with time, up-chirp), while with $D_2 < 0$ the chirp is negative (frequency decreases with time, down-chirp). For positive chirp lower frequencies have higher speed with respect to higher ones, which get delayed. For a negative chirp the situation is the opposite. As will be better explained in following chapters, pulses duration is related to temporal resolution in experiments. With this in mind, it is fundamental to investigate the temporal broadening of a pulse due to these effects.

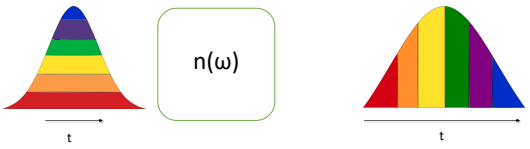

FIGURE 1.1: A compressed pulse passes through a dispersive medium ($n(\omega)$), the output pulse for the chirp theory, results in a longer pulse

1.1.2 Non Linear Processes

Linear propagation is just an approximation, in reality light propagating in a medium with non-zero second or third order polarization could give rise to non linear effects. We will limit our study to second and third order non linear effects assuming an electric field as a sum of two or three interacting waves.

$$E(z,t) = \frac{1}{2}\left[A_1 e^{\imath\omega_1 t} + A_2 e^{\imath\omega_2 t} + A_3 e^{\imath\omega_3 t} + c.c.\right] \tag{1.13}$$

To study the non-linear effects we should consider the entire polarization as follows

$$P(z,t) = \epsilon_0 \chi^{(1)} E(z,t) + \epsilon_0 \chi^{(2)} E^2(z,t) + \epsilon_0 \chi^{(3)} E^3(z,t) \tag{1.14}$$

With these assumptions, pulse propagation can be described by the following equation:

$$\frac{1}{v_g}\frac{\partial A}{\partial t} - \frac{\imath}{2} GVD \frac{\partial^2 A}{\partial t^2} + \frac{\partial A}{\partial z} = -\imath \frac{\mu_0 \omega_0 c}{2 n_0} p_{NL} e^{\imath \Delta k z} \tag{1.15}$$

where $\Delta k = k_p - k_0$, is the phase mismatch between the polarization and the field wave-vectors. Here we will discuss in detail second order non-linear processes such as sum frequency generation(SFG),difference frequency generation (DFG),second harmonic generation (SHG),optical rectification and optical parametric amplification (OPA).

1.2 Second Harmonic Generation

Second harmonic generation is a second order non-linear process in which two photons at frequency ω are absorbed and re-emitted as a single photon with frequency equal to 2ω [9, 10]. The second order term of the Equation (1.14), gives rise to a second order

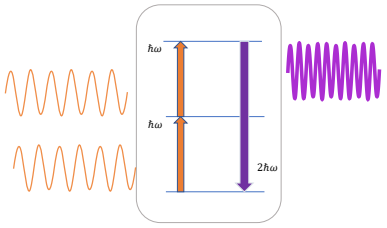

FIGURE 1.2: Scheme of beam interaction and relative energy conservation of second harmonic generation process

polarization of the type:

$$\begin{aligned} P^{(2)}(z,t) = \frac{\epsilon_0 \chi^{(2)}}{4}[A_1 e^{\imath\omega_1 t} + A_2 e^{\imath\omega_2 t} + A_1^* e^{-\imath\omega_1 t} + A_2^* e^{-\imath\omega_2 t}]^2 = \\ = \frac{\epsilon_0 \chi^{(2)}}{4}[A_1^2 e^{2\imath\omega_1 t} + A_2^2 e^{2\imath\omega_2 t} + A_1^{*2} e^{-2\imath\omega_1 t} + A_2^{*2} - 2\imath\omega_1 t + \\ + 2A_1 A_2 e^{\imath(\omega_1+\omega_2)t} + c.c. + 2A_1^* A_2 e^{\imath(\omega_2-\omega_1)t} + c.c. + \\ + 2A_1 A_1^* + 2A_2 A_2^*] \end{aligned} \tag{1.16}$$

The second order polarization gives rise to many non linear processes. Respectively noticing the second equality, the first four terms , are referred to the second harmonic generation, then the sum and difference frequency generation. The two latter terms represent the Optical rectification, however we will not spend time discussing it. By introducing the first terms into the propagation equation, and assuming a monochromatic beam with frequency ω in order to avoid group velocity dispersion, one obtains three decoupled equations

$$\begin{cases} \dfrac{\partial A_1}{\partial z} = -\imath\beta_1 A_3 A_2^* e^{-\imath\Delta k z} \\ \dfrac{\partial A_2}{\partial z} = -\imath\beta_2 A_3 A_1^* e^{-\imath\Delta k z} \\ \dfrac{\partial A_3}{\partial z} = -\imath\beta_3 A_1 A_2 e^{\imath\Delta k z} \end{cases} \tag{1.17}$$

where A_3 is the output field, $\Delta k = k_p - k_i = k_3 - k_2 - k_1$ and $\beta_i = \frac{\omega_i \chi^{(2)}}{4 n_i c}$ where $\chi^{(2)}$ is the second order dielectric susceptibility tensor. Considering that the two impinging fields are almost equal in both frequency ($\omega_1 = \omega_2 = \omega_F$ and $\omega_3 = 2\omega_F$, where ω_F is the fundamental frequency) and amplitude ($A_1 = A_2 = \frac{A_F}{\sqrt{2}}$), the (1.17) is simplified in a system of only two equations of the type

$$\begin{cases} \dfrac{\partial A_F}{\partial z} = -\imath\beta_F A_{SH} A_F^* e^{-\imath\Delta k z} \\ \dfrac{\partial A_{SH}}{\partial z} = -\imath\beta_{SH} \dfrac{A_F^2}{2} e^{\imath\Delta k z} \end{cases} \tag{1.18}$$

Equation (1.18) is then subsequently simplified through the no depletion approximation, stating that the change in the fundamental amplitude (A_F) is negligible. This approximation works properly for conversion rates around $10\% \sim 15\%$. Since the amplitude is constant ($A_F(z) = const. = A_0$), the $\frac{\partial A_F}{\partial z} = 0$ and

$$\begin{cases} \dfrac{\partial A_{SH}}{\partial z} = -\imath\beta_{SH} \dfrac{A_0^2}{2} e^{\imath\Delta k z} \end{cases} \tag{1.19}$$

whose solution is

$$A_{SH}(z) = -\imath\beta_{SH} \frac{A_0^2}{2} z sinc\left(\frac{\Delta k z}{2}\right) e^{-\imath\frac{\Delta k z}{2}} \tag{1.20}$$

This solution highlights the importance of the term Δk, the so called phase matching. Indeed, if $\Delta k = 0$ (phase matching situation), the intensity grows quadratically with respect to the length of crystal being used, allowing high conversion rates; however out of phase matching the intensity behaves as a sine function of periodicity $2L_c = \frac{2\pi}{\Delta k}$ and the peak of intensity reached is $I_{max} \approx \Delta k^{-2}$.

Phase matching

Perfect phase matching is then crucial for second harmonic generation [2]. From an ondulatory point of view during a non-linear process, new frequencies are generated locally inside the medium, and then propagate with their own phase velocity [2]. This process happens in all the longitudinal coordinates. Since the total intensity is the superposition of all these effects, when we are out of perfect phase matching, destructive interference would make all non-linear effects almost negligible. In case of zero mismatch, all components will be in phase, giving rise to a macroscopic field thanks to constructive interference. In a corpuscular point of view, phase matching can be seen as the conservation of momentum during collision of photons. The energy is conserved when $\omega_{SH} = 2\omega_F = 2\omega$, and the momentum

$$\Delta k = k_{2\omega} - 2k_{\omega} = 0 \implies n(2\omega) = n(\omega) \tag{1.21}$$

which is impossible in any isotropic medium. In isotropic media refractive index is a monotonic function of light frequency; is therefore not possible to achieve phase-matching in this kind of media as seen in figure **??** There are two methods that are

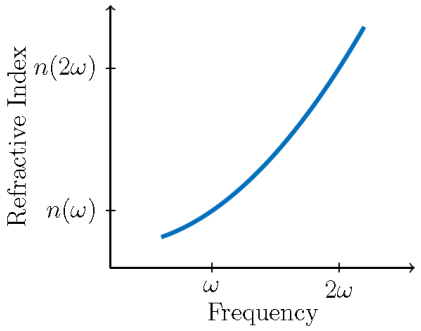

FIGURE 1.3: Refractive index of an isotropic media as function of frequency.

typically employed to achieve phase matching, the periodic poling of crystals and the use of birefringent media.The process of poling is implemented by switching periodically the sign of the dielectric susceptibility tensor. If the period is equal to twice the coherence length, second harmonic intensity will not oscillate as shown in the equation (1.20), however will keep increasing until the non-depletion approximation will no longer be valid. Whilst this approach does not allow a perfect phase match between the fundamental and harmonic (local phase matching), it nevertheless can be entirely constructive throughout the interaction length of the material and is termed quasi-phase matching (QPM)[11]. It is possible to act on the material optical properties in order to obtain a jump in phase in proximity of an intensity decreased, in order to obtain gains which can

be comparable to the phase matching situation, nas see in figure 1.4. As we can see in the graph below, we introduce a π phase shift every certain discrete distance inside the crystal, that is possibly built inverting the polarization, by the mean of electrodes, inside it. Periodic pooling crystals present a periodical susceptibility, that could be engineered properly, applying strong electric voltages.

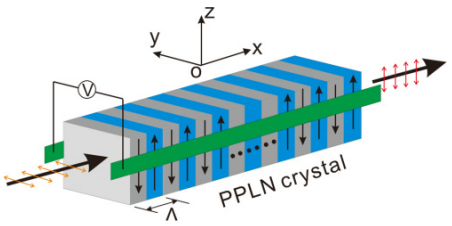

FIGURE 1.4: Periodic pooled linear crystals[11].

Since this technique is quite expensive, a valid alternative is the use of birefringent media. In these media the refractive index depends both on propagation and polarization. Uni-axial crystals for example have two different refractive indexes, extraordinary (n_e) and ordinary (n_o).The extraordinary refractive index depends on the angle between the optical axis of the crystal and the propagation direction of the beam (beam wave-vector $\vec{k}$). Uni-axial crystals can be either positive ($n_o < n_e$) or negative ($n_o > n_e$), only using a negative uni-axial crystal it is possible to tune the angle to a value for which $n_e(2\omega) = n_o(\omega)$ called phase matching angle. There are two types of phase matching, type I and II.

Negative Cr.	ω	ω	2ω
Type I	o	o	e
Type II	o	e	e

Positive Cr.	ω	ω	2ω
Type I	e	e	o
Type II	o	e	o

1.3 Optical Parametric Amplifier

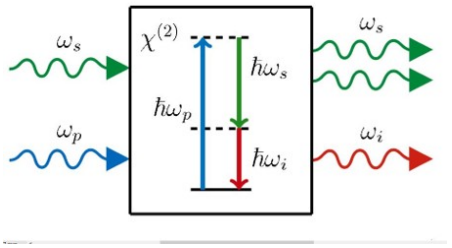

FIGURE 1.5: Optical parametric amplification by the mean of a non centro-symmetric crystal which exploits second order non linear susceptibility [12].

In most cases, frequency tunability is achieved by the second order nonlinear optical effect known as optical parametric amplification [2]. Optical parametric Amplification is a three wave mixing process where a low intensity beam with frequency ω_s called signal interacts with an high energy pump beam at frequency ω_p where $\omega_p > \omega_s$. During the process also a third beam at ω_i, called idler, is generated. The frequency relations are $\omega_p = \omega_s + \omega_i$. In alternative with respect to Difference frequency generation, here we don't have same intensity of beams, but $I_{\omega p} >> I_{\omega s}$.

1.3.1 Perfect Phase Matching

The coupled equations used to describe the propagation under the condition of second order non linear processes, are the same used in the description of OPA processes.

$$\begin{cases} \dfrac{\partial A_s}{\partial z} = -\imath\beta_s A_p A_i^* e^{-\imath\Delta k z} \\ \dfrac{\partial A_i}{\partial z} = -\imath\beta_i A_p A_s^* e^{-\imath\Delta k z} \\ \dfrac{\partial A_p}{\partial z} = -\imath\beta_p A_s A_i e^{\imath\Delta k z} \end{cases} \tag{1.22}$$

with the proper boundary conditions $A_s(0) = A_{s0}, A_i(0) = 0, A_p(0) = A_{p0}$. In order to retrieve solutions for this system it's necessary to perform two approximations.
-no depletion for pump signal ($A_p(z) = A_{p0}$)
-perfect phase matching ($\Delta k = 0$). Changing the (1.22) into the following system of coupled equations

$$\begin{cases} \dfrac{\partial A_s}{\partial z} = -\imath\beta_p A_{p0} A_i^* \\ \dfrac{\partial A_i}{\partial z} = -\imath\beta_p A_{p0} A_s^* \end{cases} \tag{1.23}$$

where, making the z derivative at both sides of the first equation, one will obtain

$$\frac{\partial^2 A_s}{\partial z^2} - \Gamma^2 A_s = 0 \tag{1.24}$$

The solution of (1.24) needs to be of the type ($A_s(z) = a_1 e^{\Gamma z} + a_2 e^{-\Gamma z}$), and applying the boundary conditions written above, it becomes

$$A_s(z) = A_{s0} cosh(\Gamma z) \tag{1.25}$$

and similarly the idler

$$A_i(z) = -\imath \frac{\beta_i A^*_{s0} A_{p0}}{\Gamma} sinh(\Gamma z) \tag{1.26}$$

Consider large gain limit ($\Gamma z \gg 1$)

$$\begin{cases} A_s(z) = \dfrac{A_{s0}}{2} e^{\Gamma z} \implies I_s(z) = |A_s(z)| = \dfrac{I_{s0}}{4} e^{2\Gamma z} \\ A_i(z) = \dfrac{A_{i0}}{2} e^{\Gamma z} \implies I_i(z) = |A_i(z)|^2 = \dfrac{I_{i0}}{4} e^{2\Gamma z} \end{cases} \tag{1.27}$$

where we could deduce the gain parameter $G(z) = \frac{e^{2\Gamma z}}{4}$. Also dividing the two intensities one can find

$$\frac{I_s(z)}{I_i(z)} = \frac{\omega_s}{\omega_i} \implies \frac{I_s(z)}{\omega_s} = \frac{I_i(z)}{\omega_i} \tag{1.28}$$

which means that for every photon of the pump absorbed, the OPA generates one photon for the seed and one for the idler, ensuring energy conservation.

1.3.2 Imperfect Phase Matching

Perfect phase matching is not always satisfied for an ultra-short pulse where many frequencies are involved, so the equation (1.23) becomes

$$\begin{cases} \dfrac{\partial A_s}{\partial z} = -\imath \beta_p A_{p0} A^*_i e^{-\imath \Delta k z} \\ \dfrac{\partial A_i}{\partial z} = -\imath \beta_p A_{p0} A^*_s e^{-\imath \Delta k z} \end{cases} \tag{1.29}$$

by following the same method used with the (1.23), one will get

$$\frac{\partial^2 A_s}{\partial z^2} + \imath \Delta k \frac{\partial A_s}{\partial z} - \Gamma^2 A_s = 0 \tag{1.30}$$

whose Ansatz is $A_s(z) = e^{-\gamma z}$.
This gives rise to

$$\imath \gamma^2 \Delta k - \Gamma^2 = 0 \implies \gamma_{1,2} = -\imath \frac{\Delta k}{2} \pm g \tag{1.31}$$

where $g(\Delta k) = \Gamma \sqrt{1 - (\frac{\Delta k^2}{2\Gamma})}$. Equation (1.29) admits solution of the type

$$A_s(z) = c_1 e^{\gamma_1 z} + c_2 e^{\gamma_2 z} \tag{1.32}$$

leading to the following equation for the light intensity.

$$I_s(z) = I_{s0}(1 + \frac{\Gamma^2}{\gamma^2}\sinh^2 gz) = I_{s0}G(z) \tag{1.33}$$

where the expression of gain parameter $G(z)$ just shown, now reduces to

$$G(z) = \frac{\Gamma^2}{4g^2}e^{2gz} \tag{1.34}$$

This formulation for the parametric gain shows that, if the phase matching condition is not achieved, the gain exponentially decreases with Δk: the higher the Δk, the lower the parametric gain.However for certain set of pump,seed and idler frequencies the matching is attained. It is indeed possible to calculate the range of frequency that could be amplified by an OPA. Let's take a set $\overline{\omega_p}, \overline{\omega_s}, \overline{\omega_i}$, and find the Δk which could amplify a band of frequencies

$$\Delta k = k(\overline{\omega_p}) - k(\overline{\omega_s} + \Delta\omega) + k(\overline{\omega_i} - \Delta\omega) \tag{1.35}$$

Expanding the terms to the first order and remembering the (1.8), the (1.35) becomes

$$\Delta k = -\Delta\omega\left(\frac{1}{v_{g\overline{\omega_s}}} - \frac{1}{v_{g\overline{\omega_i}}}\right) = -\Delta\omega\delta_{12} \tag{1.36}$$

where δ_{12} is defined as the group velocity mismatch between the signal and the idler. As long as group velocities match, phase matching can be achieved, at least to the first order. That is a very helpful condition in order to obtain a broadband phase matching and to amplify many frequencies. Ideally when $\delta_{12} = 0$, we will have $\Delta\omega \approx \infty$ that is physically impossible. In reality the approximation is inappropriate, so we should expand our $k(\omega)$ to higher order term in order to retrieve our Δk mismatch. It's possible to obtain broadband optical parametric amplification ($\delta_{12} \approx 0$) working on the geometry of our setup, in order to create another degree of freedom to solve the equation for Δk. In the collinear geometry the group velocity mismatch is equal to zero only when $v_{gi} = v_{gs}$, so when the group velocity of signal and idler are the same. Building a NOPA (Non-collinear Optical parametric Amplifier), it is possible to exploit non collinear geomertry turning the phase matching condition into a vectorial equation as follows

$$\Delta\mathbf{k} = \mathbf{k_3} - \mathbf{k_2} - \mathbf{k_1} \tag{1.37}$$

It's possible to engineer the angle between the signal and the idler, in order to have phase matching when $v_{gs} = v_{gi}cos(\alpha)$ where α is the angle between signal and idler beams. This shows that, as in the collinear case, broadband amplification is obtained when the group-velocity of the signal matches the projection of the group velocity of the

idler along the signal direction. It's important to notice that this is possible only if the envelope of the idler travels faster than the signal one ($v_{gi} > v_{gs}$).

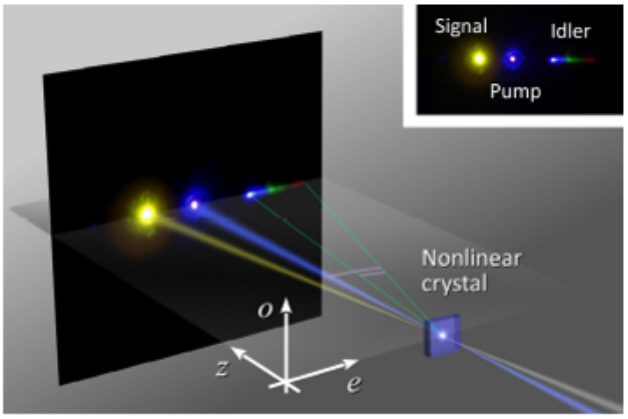

FIGURE 1.6: Non-collinear OPA configuration,exploiting the angle between the three beams [2]

1.3.3 NOPA Setup Development

The development of the setup for a Non-collinear Optical parametric amplifier fundamentally consists of three subsystems
- the seed generation
- the parametric amplification
- A pulse compression stage to obtain the Transform Limited pulse at output of OPA.

Analyzing the operation of these three blocks provides the key for understanding the properties of the OPA and in particular the design required to achieve specific working parameters [2]. This multi-stage approach permit us to control very precisely the Group Velocity mismatch between the pump and the seed in order to achieve a broadband amplification. Moreover it is able to adjust the pump intensity which is strongly linked to the parametric gain that will be obtained. In the seed generation stage, the process of white light generation occurs by mean of third order non-linear susceptibility, $\chi^{(3)}$, effect obtained focusing the laser beam into a dielectric crystal. The best solution is to use un-doped sapphire which, due to its very high thermal conductivity and damage threshold, guarantees excellent stability and damage-free operation. This effect of white light continuum generation induces a parabolic frequency chirp and a dramatic spectral broadening. The second stage is the actual Parametric Amplification. The white seed is amplified making it interact with the monochromatic pump pulse. In order to optimize this process, one should carefully adjust the pump-pulse (wavelength, energy and duration) and the nonlinear interaction (crystal Type and crystal length)

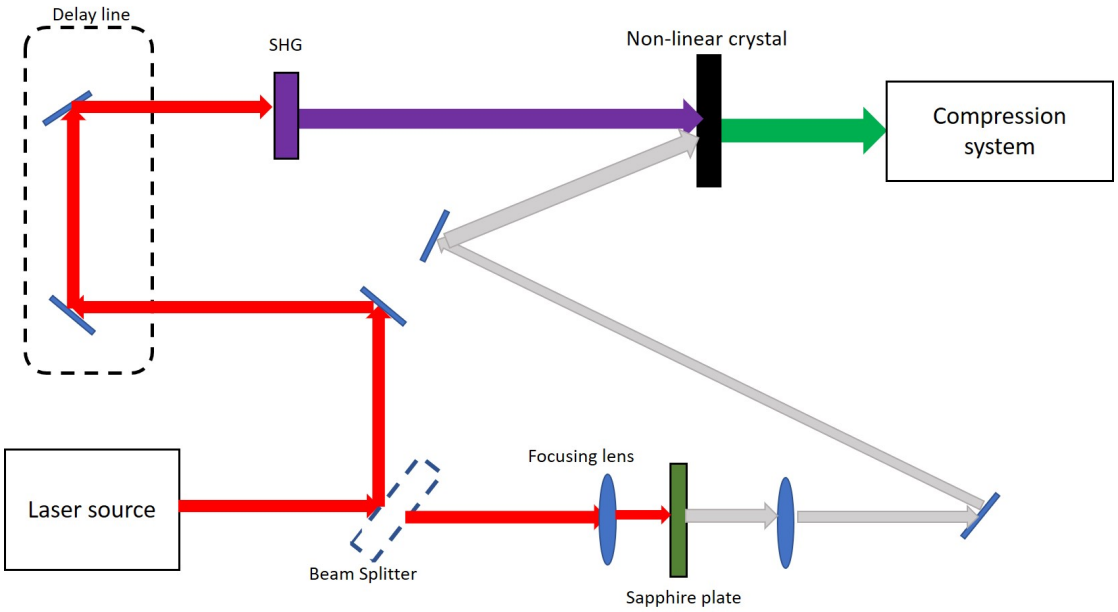

FIGURE 1.7: Block scheme Setup for an ultrafast non-collinear OPA, where SHG: second harmonic generation

parameters. Because of that the pump pulse is suitably delayed by the use of a delay line or delay stage, in order to match different frequencies of the chirped white light continuum. This occurs because the amplification process happens only when the seed and the pump are overlapped spatially and temporally. Furthermore the parametric gain is strictly dependent on the pump energy or intensity. Generally, a very high peak intensity may start spurious nonlinear interactions, such as undesired cascaded second order processes among pump, signal and idler beams, or third order processes such as self phase-modulation, self-focusing and small-scale filamentation. In addition, high intensities may damage the surface of the crystal [2]. In order to avoid these it is helpful to have a clean beam profile. When designing an OPA, we need to carefully control the nonlinear interaction parameters. The first crystal parameter that should be taken into account is its transparency range because this determines the tunability range of the OPA. Finally the compression stage is made by an integer number of reflections on dielectric chirped mirrors, which help to compensate the group delay and the third order dispersion. In the figure 1.7 we can see a scheme for an experimental setup which is capable to obtain very energetic pulses within a Transform Limited duration around $10fs$, in the visible and near infrared region of frequencies.

1.4 White light generation

This third order non linear process refers to an extreme broadening of the pulse, by mean of a crystal (generally Sapphire or CaF_2) Here we discuss the main processes behind

this phenomenon.

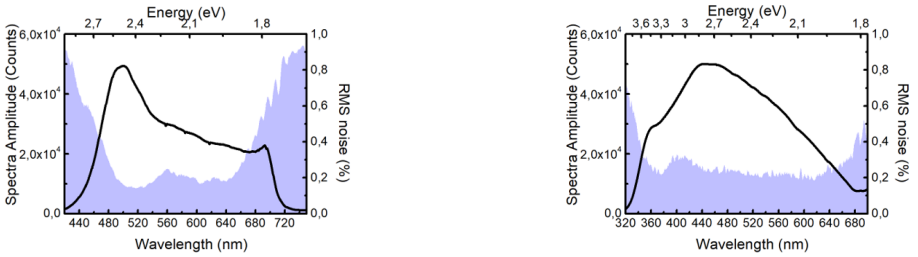

FIGURE 1.8: White light generation spectra, revealing frequency dependent spectral amplitudes and relative noise fluctuations using Sapphire Al_2O_3 (on the left) or calcium fluoride CaF_2 (on the right)[13].

1.4.1 Four Wave Mixing

Consider a three wave field with different frequencies and wave vectors as in equation (1.13) impinging on a crystal. Third order non-linear polarization can be expressed as:

$$P_{NL}^{(3)} = \frac{3}{8}\epsilon_0 \chi^{(3)} A_1 A_2^* A_3 e^{\imath(\omega_1 - \omega_2 + \omega_3)t - (k_1 - k_2 + k_3)z} + \dots \tag{1.38}$$

In order to study the generation of white light only one frequency and one intensity is needed ($\omega_1 = \omega_2 = \omega_3 = \omega$ and $A_1 = A_2 = A_3 = A$) Expression (1.38) simplifies to

$$P_{NL}^{(3)} = \frac{3}{8}\epsilon_0 \chi^{(3)} |A|^2 A e^{\imath(\omega t - kz)} \tag{1.39}$$

It is interesting to notice that this effect depends on the intensity of the field, so could be negligible for very low intensities. Inserting this polarization term in the (1.15),

$$\frac{\partial A}{\partial z} + \frac{1}{v_g}\frac{\partial A}{\partial t} - \frac{i}{2} GVD \frac{\partial^2 A}{\partial t^2} = -\imath\gamma |A|^2 A \tag{1.40}$$

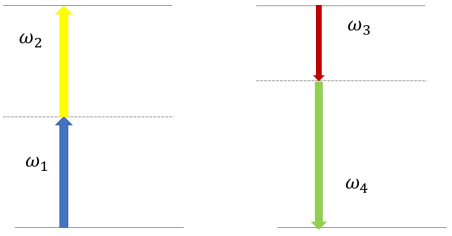

FIGURE 1.9: Scheme for the energy conservation during a four wave mixing process

where $\gamma = \frac{3\chi^{(3)}}{16 n_0 c}$. The first order time derivative can be removed by a change of coordinates ($z' = z \; and \; t' = t - \frac{z}{v_g}$), leading to:

$$\frac{\partial A}{\partial z} - \frac{\imath}{2} GVD \frac{\partial^2 A}{\partial t^2} + \imath\gamma |A|^2 A = 0 \tag{1.41}$$

This four wave mixing process, exploiting non linear effects of the third order introduces a lot of new frequencies in the pulse spectrum.

1.4.2 Self phase modulation

Self Phase modulation could be investigated by a comparative analysis of several numerical methods operating either in time or frequency-domain. Numerical results show that self-phase modulation phenomena can occur when the optical power is sufficiently high. [14].

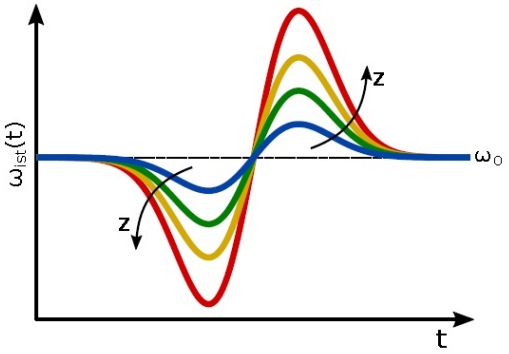

FIGURE 1.10: Instantaneous frequency generation in a $\chi^{(3)}$ crystal.

Let's suppose a material with negligible group velocity dispersion ($GVD \approx 0$), the equation (1.41)could simplify as

$$\frac{\partial A}{\partial z} + \imath\gamma |A|^2 A = 0 \tag{1.42}$$

An ansatz for the solution could be that propagation only affects the phase of the field

$$A(z,t) = A(0,t) e^{-\imath \Delta\varphi_{NL}(z,t)} \tag{1.43}$$

This could be acheived using separation of variables in (1.42) and assuming intensity constant ($A(z,t) \implies A(0,t)$), obtaining

$$A(z,t) = A(0,t)e^{\imath(\omega_0 t - kz - \overbrace{\gamma|A(0,t)|^2 z}^{\Delta\varphi_{NL}})} \tag{1.44}$$

The istantaneous frequency can be obtained by the first derivative of the phase term in the (1.44)

$$\omega_{ist} = \frac{\partial\varphi(z,t)}{\partial t} = \omega_0 - \gamma z \frac{\partial|A(0,t)|^2}{\partial t} \tag{1.45}$$

Considering a Gaussian temporal profile of the intensity the shape of the frequency in time will be as shown in the following figure. As one can see the propagation broadens the spectrum symmetrically towards the blue and the red. The spectral broadening linearly depends on the thickness of the crystal: the thicker the crystal, the broader the white light is.

Chapter 2

Pump-Probe Spectroscopy

Pump probe spectroscopy is a widely used ultrafast spectroscopic technique which provides valuable information on the nature and dynamics of photo-generated species in solids and molecules. A major application of ultra-short light pulses is for time-resolved studies of ultra-fast dynamical processes in chemical, solid-state, and biological materials. Just as high-speed (microsecond)light flashes have been used for many decades to make stop-action photographs of rapid (microseconds and slower) mechanical motions of macroscopic objects, ultra-short laser pulses are a unique tool for excitation and stop-action measurements of ultra-fast microscopic and quantum mechanical processes within materials [15]. The principle scheme of a femto-second pump probe setup is presented in figure 2.1, where an energetic pulse resonant with an electronic or molecular transition, the pump, is followed by a second pulse, referred as probe which tests the new system after the creation of a population difference. The probe impinging after a delay T with respect to the pump, generates the third order polarization which radiates a field

$$E^{(3)}(0,T,t) \cong \imath P^{(3)}(0,T,t) \tag{2.1}$$

However, since the measurement is done by comparing the signal whenever the pump is transmitted or not, we need to modulate the pump with an optical modulator (chopper).

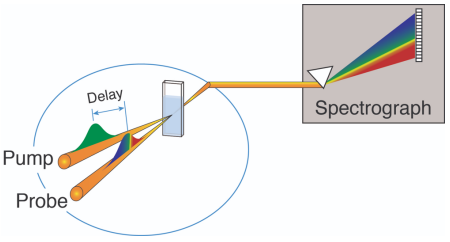

FIGURE 2.1: Generic non-collinear Pump-probe spectroscopy scheme

Once the pump is off, one gets at the detector the probe energy

$$U_{OFF} = \int_R |E_{probe}|^2 \, \mathrm{d}t \tag{2.2}$$

On the other hand when the pump is switched on

$$U_{ON} = \int_R |E_{probe} + E^3(0, T, t)|^2 \, \mathrm{d}t \tag{2.3}$$

. Then the measured signal is of the type

$$\frac{\Delta T}{T} = \frac{U_{ON} - UOFF}{U_{OFF}} \tag{2.4}$$

2.1 Theory

Let us first consider a situation in which a sample is illuminated by two beams, the first, the pump pulse is centred at time zero with an intensity profile $I_{pu}(t)$, than the second is centred at a delay τ following an intensity function of the type $I_{pr}(t-\tau)$. Furthermore, we assume that a fraction of the probe is transmitted as in figure 2.1. Calling α the linear absorption of the material used as sample, the pump beam induces a difference in the absorption of the type

$$\Delta\alpha(t) = \int_{-\inf}^{t} I_{pu}(t')A(t-t')\mathrm{d}t' = I_{pu}(t) * A(t) \tag{2.5}$$

which is a convolution product. The $A(t)$ function is the impulse response of the medium that should be determined. Moreover the change in the transmitted probe pulse intensity is

$$\Delta I_{pr}^{tr}(t) = I_{pr}(t)exp(-\alpha_0 d)[exp(-\Delta\alpha(t)d) - 1] \cong -I_{pr}(t)exp(-\alpha_0 d)(-\Delta\alpha(t)d) \tag{2.6}$$

where α_0 is the linear absorption coefficient and d is the medium dimension, along the wave propagation axis, and we supposed the perturbation being small ($\Delta\alpha d \ll 1$), in order to get an approximated behaviour easier to study [15]. Finally the pump induced variation of transmitted probe energy is

$$\Delta U_{pr} = A(t) * C(t) = A(t) * [I_{pu}(t) \otimes I_{pr}(t)] \tag{2.7}$$

where $C(t)$ is the cross correlation between the pump and probe intensity profiles. The $C(t)$ which appears in the equation (2.7), also known as impulse response function, determines the maximum resolution of our pump-probe experiments. The last equation convinces us to use short pump and probe pulses in order to resolve dynamics of fast

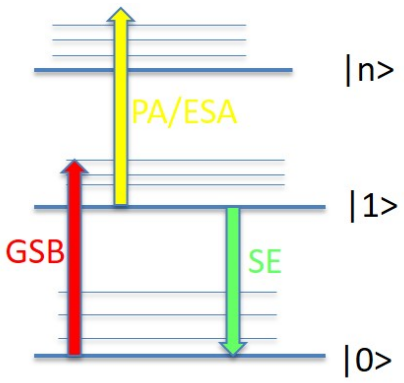

FIGURE 2.2: Possible signals obtainable from the Pump-Probe spectroscopic experiment Ground-State-Bleaching (GSB),Stimulated-Emission (SE),Photo-Absorption (PA) or Excited-State-Absorption (ESA)

processes. All the processes that are faster than the cross correlation are averaged out and can not be detected in a proper way. For delays τ much longer than the duration of the cross-correlation, the case of well-separated-pulses, it is possible to retrieve the energy of the transmitted probe through a sample ΔU_{pr}^{tr}, and it is possible to calculate the differential transmission as follows

$$\frac{\Delta T}{T} = -\Delta\alpha d \tag{2.8}$$

From the equation above we can notice how the differential absorption and transmission are strongly linked and are opposite to each other. Both the differential transmission and the differential absorption are functions of probe frequency and delay. $\frac{\Delta T(\omega_{pr},\tau)}{T}$, $\Delta\alpha(\omega_{pr},\tau)$. From now on let's focus on the absorption change induced by the probe beam. Considering n electronic states with populations N_i which the pump beam changes by an amount ΔN_i. One can then write

$$\Delta\alpha(\omega_{pr},\tau) = \sum_{i,j=0}^{n} \sigma_{ij}(\omega_{pr})(\Delta N_i(\tau) - \Delta N_j(\tau)) \tag{2.9}$$

where σ_{ij} is the frequency dependent cross section for the transition from the N_i to N_j. To understand possible signals deriving from the Pump-Probe experiment let us first refer to the figure 2.2, in which are present three different energetic levels, the ground level $|0>$, and two excited states $|1>$ and $|n>$ each one with its vibrational transitions. In order to understand the transient processes in this system it is necessary to approximate the pulses as well separated, so they refer to a time scale longer than the resolution of our system (cross-correlation).

Ground State Bleaching

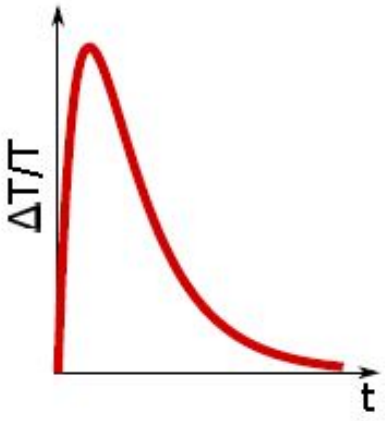

FIGURE 2.3: Possible $\frac{\Delta T}{T}$ Ground State Bleaching dynamics

In a 3-level system,pump pulses are resonant to $|0> |1>$. From the measurement one notices a positive signal decaying with the lifetime of $|1>$, as we can see from figure 2.3 . This happens because the pump is absorbed, exciting the system and depleting the ground state. The probe, resonant to the other transition from the ground state, should get absorbed, however there is no population in the fundamental state, therefore the sample is more transparent to the probe radiation and its transmission increases. While the pump is off the probe is absorbed: the signal is positive and can provide information about the first excited state ($|1>$) lifetime [16].

Stimulated Emission

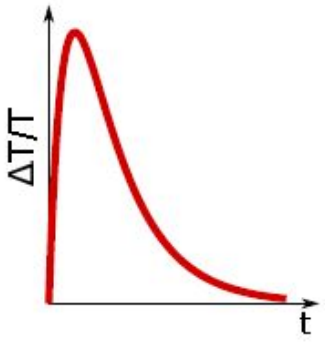

FIGURE 2.4: Possible $\frac{\Delta T}{T}$ dynamic for stimulated emission

Let us now consider a situation in which the probe frequency is slightly smaller than the pump one ($\hbar\omega_{pump} > \hbar\omega_{probe}$). This means that when the pump triggers the $|0>$ to

$|1>$ transition, the probe could provoke the stimulated emission of photons with similar wavelength with respect to the pump, reaching an upper vibrational level on the ground state. The final state energy will be $E = \hbar\omega_{pump} - \hbar\omega_{probe}$. This will give rise to an increase in the differential transmission ($\frac{\Delta T}{T} > 0$), which allows us to study the lifetime τ_1 of the excited state $|1>$.
It's important to notice that the Ground State Bleaching and the Stimulated Emission signals could overlap with each other, creating many difficulties to distinguish between them. To better understand which phenomenon occurs it is necessary to deeply know the orbital molecular behaviour: for instance via density functional theory (DFT).

Excited State Absorption

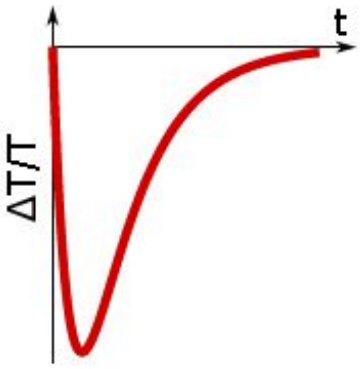

FIGURE 2.5: Possible $\frac{\Delta T}{T}$ dynamic for excited state absorption signal

The excited state absorption is a peculiar feature of a two-colour pump-probe experiment. With a degenerate pump-probe experiment, in which pump and probe beams share the same frequency, it's impossible to observe transitions to higher energetic levels. When the pump is off, the first excited state is not populated and so the sample is transparent with respect to the probe. Although when the pump collides the sample, it promotes some electrons to the $|1>$ state and now the probe could be absorbed by the sample. It will clearly result that in this case, differently from the other two signals, one will obtain a negative signal in differential transmission. A final, important note is related to the trade off between isolating a particular phenomenon and measuring accurately the time constant associated with the transition under study. This comes from the fact that fine control over the delay between the pump and probe directly influences time resolution but the lower limit is imposed by the instrumental response function, intrinsically correlated to the duration of the pulse. This means that, in order to resolve fast dynamics, short pulses are required[17],but due to the Fourier theorem, short pulses are broadband pulses, which will trigger transitions different form the one under study.

This means that in such experiments it is not possible to get both selectivity on the excited transition and the temporal resolution.

2.2 Broadband Pump Probe

Many setup configurations are possible in order to exploit pump probe spectroscopic technique. The two beams can share the frequency, if they come from the same laser or optical parametric amplifier. The signal depends only on the delay between these two pulses τ; this configuration is called **Degenerate pump-Probe**. It's not possible to detect pump induced absorption or the creation of new excited state in the molecules with a simple degenerate pump-probe experiment, but we need at least two different frequencies for the pump and the probe: this is called **Two-colour pump-probe**. In order to study all the possible photo absorption signals it is useful to have a broadband probe to detect absorption of all possible frequencies (**Broadband hyper-spectral pump-probe**). In figure 2.6, it's possible to see the block scheme of a broadband pump probe, starting from a coherent laser source (titanium sapphire, at 1kHz repetition rate). The pump is ultra-short in time to obtain a very high resolution and is generated by a tunable parametric amplification of a certain region of frequency, usually between $500 - 700nm$. The pump beam needs to be focused onto a sample where it needs to overlap spatially and temporally the probe beam in order to perform pump probe spectroscopy. Moreover the pump is modulated using a mechanical light chopper, which is linked with the electronic detection system by the mean of a Lock-In amplifier (LIA). In addition to modulating the light source, the chopper also provides a synchronous reference signal capable of driving the reference channel of a lock-in amplifier. This reference output voltage is a square wave, usually in the order of a few volts peak to peak. The probe instead is generated by white light continuum generation which exploits non-linear effects of the third order. This non linear effects involves third order susceptibility, $\chi^{(3)}$, so we can use centro-symmetric crystals ($\chi^{(2)=0}$). Note that the performances of the pump-probe ultimately rely on the white light continuum generation, which is employed both for the generation of the broadband probe pulse and of the seed of the non-collinear OPA [18].

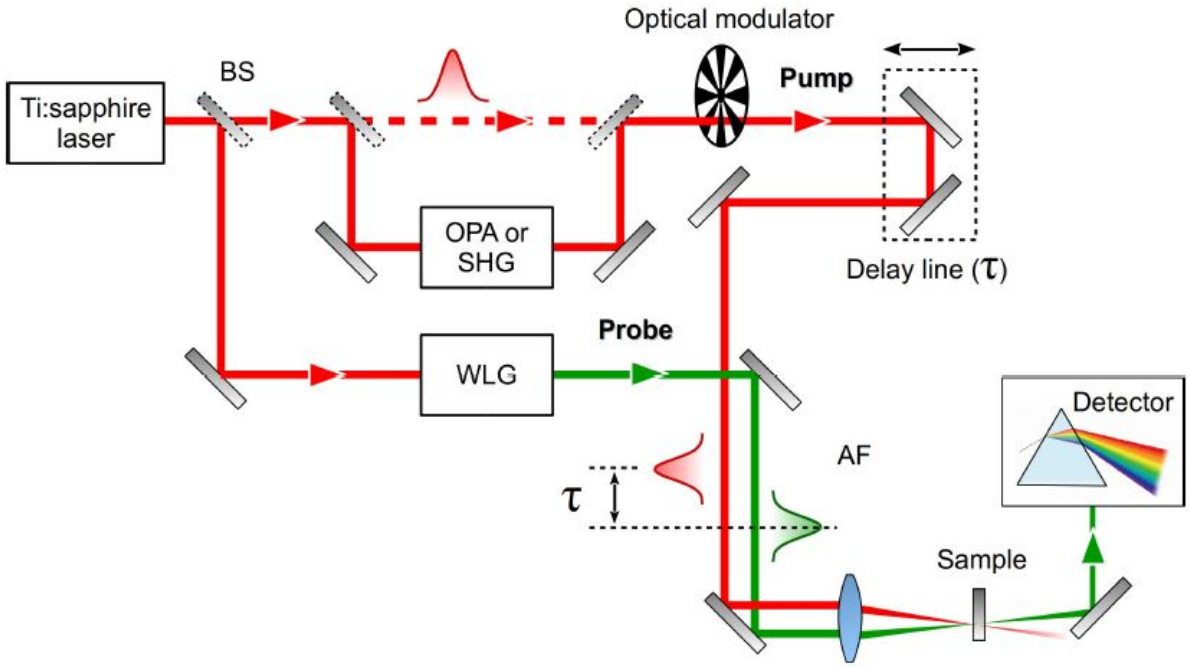

FIGURE 2.6: Experimental setup configuration for a broadband hyper-spectral pump probe [18]

Chapter 3

Experimental Setup

In this chapter will be presented the experimental setup used to perform pump-probe spectroscopy, pumping in the Ultraviolet region.
Analyzing all the components of this setup, it will be possible to understand all the issues and difficulties encountered to fill the requirements for the experiments and methods to overcome these will be suggested. As could be seen from the figure 3.1 the laser beam is split to create two different branches, which are responsible of pump and probe generation. the two beams after recombine, spatially and temporally overlapped to each other, and collide on a sample to investigate probe differential transmission at the output with an optical multichannel analyzer. The differential transmission is measured when we modulate the optical pump beam by an optical chopper which is linked to the spectrometer and refers to the spectrometer itself when the pump is transmitted or So it is able to measure intensity and frequency of modulated signal and then communicates with the spectrometer in order to retrieve the differential transmission. The laser source employed in this thesis is a Libra (Coherent) providing $4\,mJ$, $100-fs$ pulses at a central wavelength of $800\,nm$ with a repetition rate of $1kHz$. A fraction of $500\,\mu J$ is used to pump the whole setup. The laser output polarization is horizontal, but becomes vertical before entering in the setup by means of a periscope. The beam is split to create the two branches initially, the pump and the probe. The requirements for performing this experiment are basically two:

1. obtaining an ultrashort pulse used as pump, which generally should be a $sub-20fs$ light pulse in order to have optimal resolution.

2. creating a broadband probe both in the Visible and Ultra-violet range in order to obtain all the possible transient signals deriving from pump excitation.

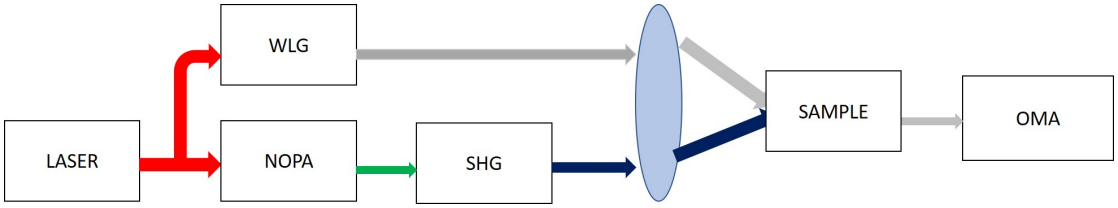

FIGURE 3.1: Block diagram of the experimental setup.

3.1 Ultra-Short pulses generation in the Ultraviolet region

Since the biological samples absorb in the UV range this setup delivers tunable UV pulses through second harmonic generation from the broad visible spectrum generated from an OPA.

Tunable ultra-short pulses generation (Broadband NOPA)

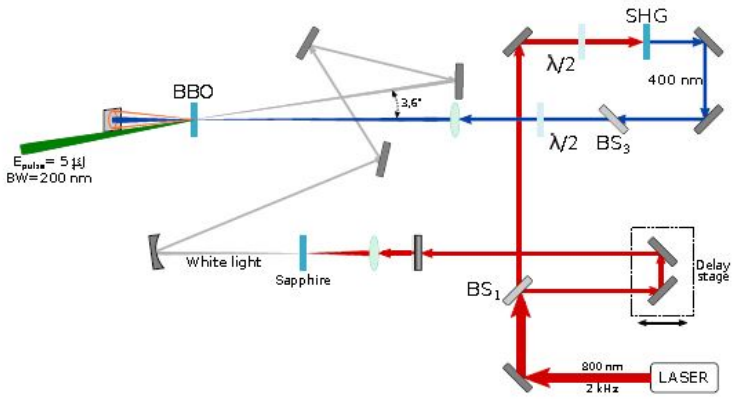

FIGURE 3.2: Non-collinear Optical Parametric Amplifier setup; the crystal used for SHG is a type-I BBO [13].

The first step is to generate visible broadband pulses by the mean of a non-collinear OPA. Around 10% of the laser light is sent trough a Sapphire crystal to generate white light which provides the seed radiation to the NOPA. The stability of this white light is crucial, because eventual fluctuation will be amplified through the process.
The remaining 90% of the light is sent through half-wave plate to rotate its polarization by 90° and frequency doubled through SHG in a type I $1 - mm$ thick BBO crystal (Barium Borate Ba_2BO_3)cut at 29.2°. The fundamental radiation ($800nm$) is removed

thanks mirrors which are transparent to that frequency and highly reflect the second harmonic frequency range (around $400nm$). Both the pump and the seed are focused onto another BBO $1 - mm$ thick and 32 cut. From theory it is known that the optimal angle between the beams to achieve broadband phase matching is 3.6° [2]. Time synchronization is achieved by a manually operated delay stage capable also to tune the central wavelength of the output spectrum in the visible range $(500 - 700nm)$. This tuning is possible because the seed of the OPA is strongly chirped by mean of white light generation ($\chi^{(3)}$ processes).

Then the output beam is compressed using a pair of chirped mirrors (12 reflections),

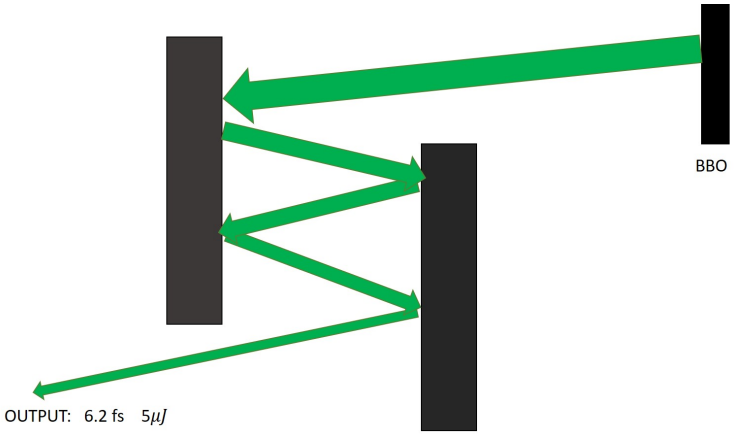

FIGURE 3.3: Compression system made by the use of chirped mirrors.

which introduce a negative group delay dispersion for each bounce (see figure3.3). So far, at the output we will obtain short pulses ($6.2fs$ transform limited) with energy around $5 - \mu J$ as seen in figure 3.4.

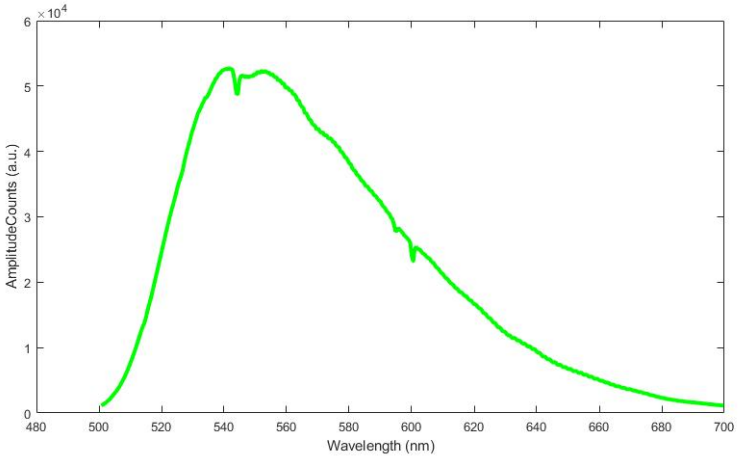

FIGURE 3.4: Spectrum at the output of a visible NOPA, after the chirp mirrors compression

Tunable Ultra Violet Pulses

It is very useful to obtain tunable ultra-short pulses in the visible or Infra-red frequency region. Many rapid molecular dynamical processes have been investigated using broad-band pump pulses very short in time in order to obtain high temporal resolution systems. Experiments have been performed to study graphene and other low dimensional materials [19] or Rhodopsin, the eye protein.[20]
It is important to remember that our need is to study biological samples, like amminoacids and proteins, which present a benzenic ring with strong absorption in the UV. In other words our goal is to produce ultra-short pulses in the ultraviolet region, to be used as pump pulses for our pump-probe spectroscopic experiment, because as we noticed above the duration of the pulse directly affects the temporal resolution of the measurement: in a pump probe measurement temporal resolution is limited by the correlation between the pump and the transform limit of the probe.[20]
However it is very problematic to generate tunable UV pulses starting from a visible OPA, because many issues occurs.

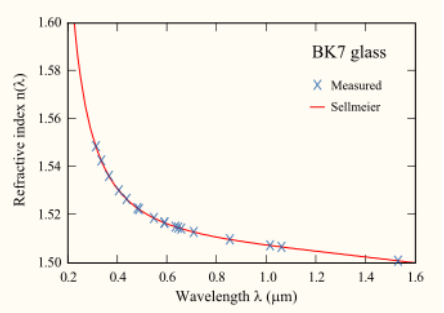

FIGURE 3.5: Refractive index as a function of frequency in crown glass (BK7 glass)[21].

The first difficulty is to find crystals with suitable refractive indices in the UV. In the picture 3.5 it's clear how the frequency dependent refractive index $n(\omega)$ of crown glass, used for most lenses and mirrors, becomes very high with increasing input frequency, and this is similar for most of commercial materials.
Moreover the parametric amplification process could be hampered by two photon absorption. Pumping the seed to have UV output pulses needs very high energetic pump pulses, inducing the material to absorb more than one photon at a time. This prejudices a lot the seed amplification and the possibility to obtain energetic and short output pulses.
Finally is very difficult to control UV pulses spectral phase; this limits a lot the possibility to obtain transform limited pulses as output of a NOPA. Chirp mirrors, in fact, are not good anymore because they present a trade-off in the ultraviolet region between

reflectivity and group delay dispersion (GDD). It is indeed very difficult to obtain UV pulses at the output of chirped mirrors having both high energy and low group delay dispersion.

Having become aware of all these issues, our method to solve these troubles is to add a second part in our setup. After the generation of visible transform limited ultra-short pulses, the output beam will be frequency up-converted, by means of another type I BBO crystal which exploits second harmonic generation, as we can see from the figure 3.6.

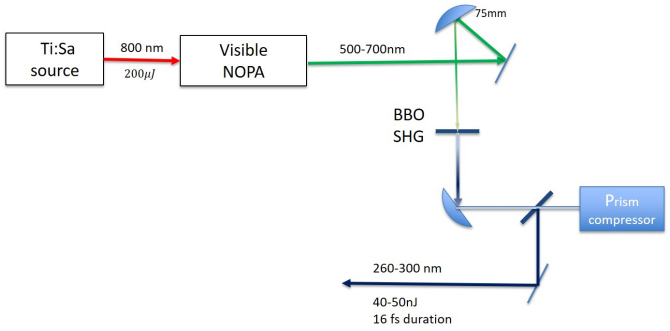

FIGURE 3.6: Frequency up conversion through SHG in order to obtain ultra short pulses in the Uv overcoming all the difficulties explained.

The frequency doubled output beam is then compressed through a prism pair compression system. This prism pair (figure 3.7) has two functions, block the fundamental beam

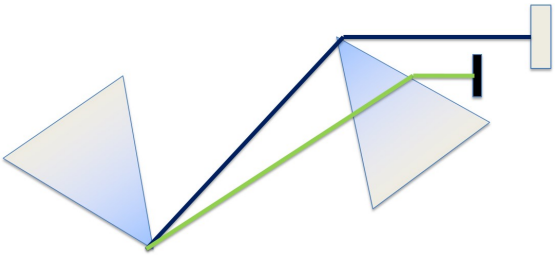

FIGURE 3.7: Prism pair for compression of the UV pulse, the fundamental component is absorbed and the others will be shortened in duration.

coming from the NOPA, and compress the second harmonic signal to obtain transform limited pulses. They are able to introduce a negative group delay dispersion ($GDD < 0$). The prisms are both made of Magnesium Fluoride (MgF_2), and lay at a fix distance $215mm$ long. Moving the second prism along the perpendicular plane with respect to the beam propagation, we can shorten or increase the optical path, while the geometrical one remains unchanged. The impinging angle should be the Brewster angle, in order to transmit all the p-polarized light which comes from the BBO.

As a matter of fact, with the entire setup is possible to obtain output pulses in the UV

frequency range (between $260 - 300$ nm), with a suitable duration (around $16fs$ TL), and energy ($40 - 50nJ$). This ultra-short transform limited pulse will be used as UV pump for our pump-probe spectroscopy experiment.

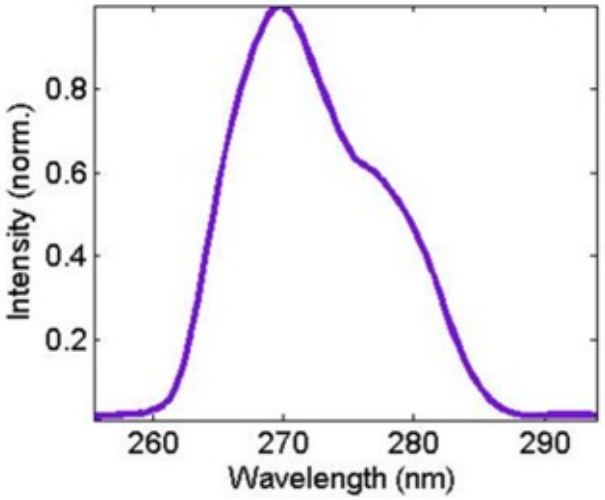

FIGURE 3.8: Example of pump pulse, deriving from the UV generation part of the experimental setup

In the pump-probe spectroscopy the time resolution is determined essentially by the duration of the pump pulses[17]; for that reason it is crucial to characterize precisely its time profile. We need to both know the spectral amplitude and phase and with the spectrometer it is possible to get the spectral amplitude only. One of the best technique to retrieve spectral phase in the UV range is a modified scheme of two-dimensional spectral shearing interferometry (2DSI). This interferometric technique consists of two ancillae pulses sheared by a frequency Ω, and delayed by τ_{CW}. With the precise controlled scanning of τ_{CW} and the possibility to have a direct measurement of Ω via spectrometer, the spectral phase, function of frequency $\phi(\omega)$, can be calculated starting from the intensity profile of the interference pattern between the two replica.

3.2 Broadband pulse generation for probe

In a pump-probe experiment the probe is usually a weak energy broadband pulse mapping the whole spectral region where electronic transitions happen. Since the purpose of our experiment is the study of biomolecules in the visible and ultraviolet region, we need probe white light continuum pulses spanning between $300 - 700$ nm. White light generation is a process taking place in Kerr media and primarily triggered by self phase modulation [22]. As shown in the previous chapters, the white light generation phenomenon is associated with the $\chi^{(3)}$, and could appear in any material if the beam intensity is high enough. The probe is then focused on the sample with a spot-size around 100x100μm^2, and energy roughly $1\mu J$.

Visible white light generation

In our experimental setup, for reasons regarding the stability of the generated white light, only Sapphire or calcium fluoride are used to exploit third order non linear effects [23]. They are more fragile than other crystals, like YAG (yttrium aluminum garnet) which has a very high damage threshold, but they present less fluctuations in the continuum, so less noise.
One important feature is the possibility to adapt the setup configuration in order to obtain white light both in the visible and in the ultraviolet region of the spectrum. It's better to start discussing the visible white light; starting from the setup configuration described in the figure 3.11, it can be seen how fundamental light coming from the laser source ($800nm$) is focused on the crystal by a converging lens ($f = focal\,length = 50mm$). Then the beam collides onto the crystal plate and produces white light, starting from 400 up to nearly 800 nm frequency range. A BG39 short-wave-pass filter is used to

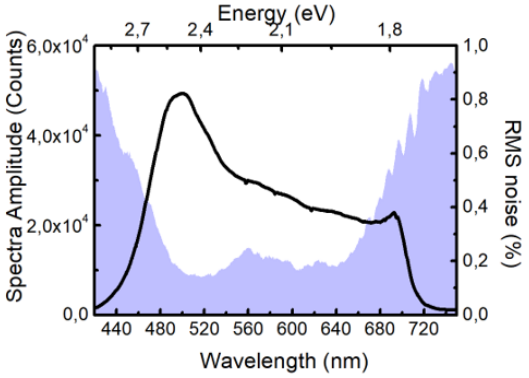

FIGURE 3.9: White light spectrum with noise fluctuations created using a Sapphire crystal.

cut off the remaining fundamental light from the laser. The BG39 is a short-pass filter

for ultra-fast pulses, which cut off wavelength longer than 700 nm. The resulting output spectrum, as shown in figure 3.9, is very stable in terms of noise fluctuations (RMS noise about $0,2\%$ over the whole range).

Using the calcium fluoride (CaF_2), the situation is slightly different. Firstly the spectrum is broader, covering a bigger range from 320 up to 700 nm. Alternatively to Sapphire the CaF_2 crystal has lower damage threshold in terms of impinging beam intensity, so it can not be exposed to laser light for more than few seconds in the same point.It is therefore necessary to slowly move the crystal, causing noise to increase. In this case two linear motorized stages (Zaber Technologies, model T-LS28M), mounted in order to slowly scan the plate in a plane perpendicular to the propagation direction [12], have been programmed to move the crystal in a spiral-like way. For such reason the measurements using probe obtained with CaF_2 are two times noisier than the measurements obtained with Sapphire generated white light continuum.

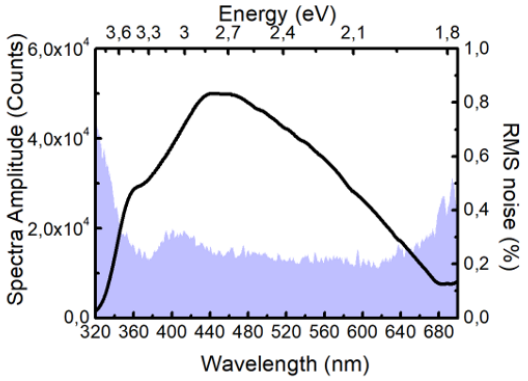

FIGURE 3.10: white light spectrum with noise fluctuations created using CaF_2 crystal

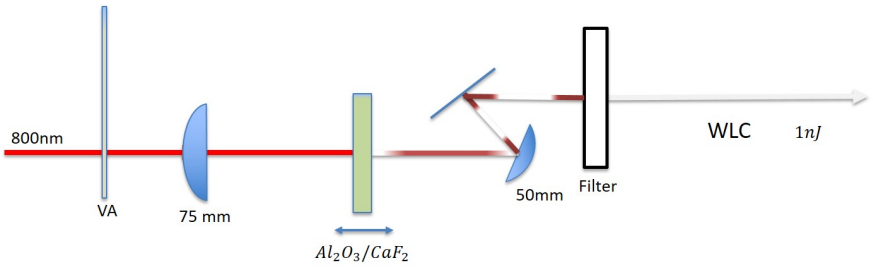

FIGURE 3.11: Block scheme for the generation of white light in the visible region. VA:Variable Attenuator

Ultra-Violet white light generation

Biomolecules have photo-absorption very spread along visible and Ultraviolet frequencies, so it's useful to study their dynamics and transient spectra in the UV region of

light. One possibility is to widely increase the transmission spectrum of the probe, creating ultraviolet white light which is useful to detect higher energy transitions. The Setup configuration slightly changes with respect to the visible white light generation, the beam before being focused on the crystal, passes through a BBO crystal which exploits the non linear effect of second harmonic generation. After doubling the frequency the beam is then focused onto a CaF_2 crystal which produces white light into the ultraviolet region. This white covers a wavelength range between 240 and 380 nm, as can be seen in figure 3.12 It is not possible to use sapphire plate to obtain UV white

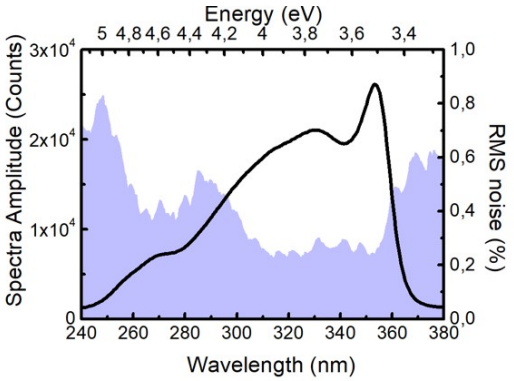

FIGURE 3.12: White light spectrum generated by a CaF_2 after the fundamental has been doubled in frequency

light because the sapphire is highly absorbing in that region. Being transmitted from the crystal the probe beam passes through two filters instead of one that are capable of filtering the remaining fundamental component and the 400 nm (second harmonic frequency component).

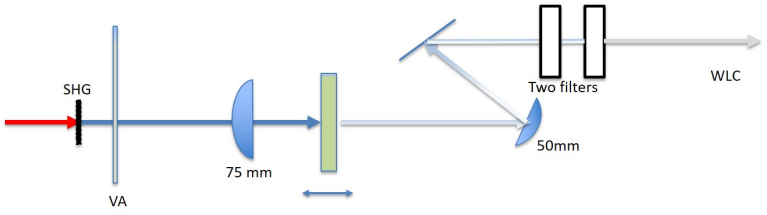

FIGURE 3.13: Setup scheme for the generation of broadband probe in the ultraviolet region

Effective temporal resolution with strongly chirped probe pulses

Femtosecond pump probe spectroscopy is widely used to analyze transient spectra of fast processes which appear in nature, as explained in the previous chapter. So the temporal resolution needs to be very high in order to detect these processes. With the goal of improving the temporal resolution, a great effort has been devoted to the generation of

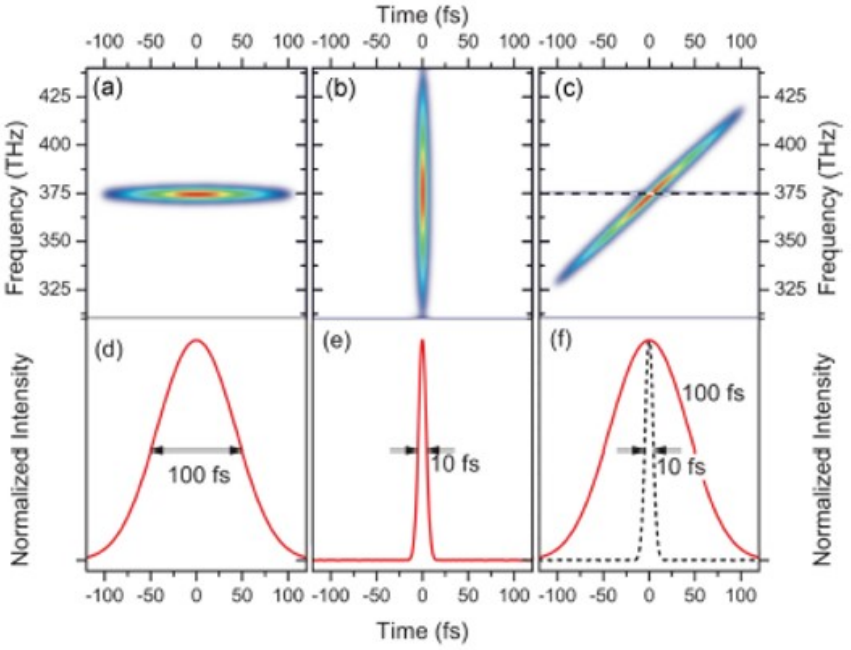

FIGURE 3.14: (a-c) WSs of three pulses with a $375 - THz$ carrier frequency: two TL Gaussian pulses, $100 fs$ (a) and 10 fs (b) in duration, and a strongly chirped pulse with a pure quadratic phase (group delay dispersion, GDD = $360 fs^2$), causing a temporal broadening up to a spectrally integrated duration of 100 fs (c). (d-f) Temporal profiles obtained by spectrally slicing the three pulses at their central frequency; the dashed line in (f) represents the corresponding spectrally-integrated pulse temporal profile.[25]

ultrabroadband light pulses and to their compression to the transform-limited duration, down to just a few cycles of the carrier wavelength.[24] In our experiments we assume that the temporal resolution of our system is the impulse response function (IRF), of the instrumental configuration. As derived from the theory, the IRF of a pump probe measurement is the cross correlation between the pump and the probe intensity profiles. It has been shown how the pump beam is compressed with multiple reflections on double chirp mirrors; referring to the probe this doesn't happen. Moreover the broadband probe generated through white light continuum in a bulk crystal is a common tool for pump probe spectroscopy, but has a lot of frequency chirp. It can be shown that for a chirped WLC probe pulse one can recover the temporal resolution of the corresponding nearly transformed limited pulse, provided that the probe pulse is detected through a narrow-band filter [25] This has the advantage to avoid setting up a pulse compression system with proper wavelength dependent negative GDD. The wavelength dependent zero time will be determined with a proper MatLab code. Then, the time-corrected transient signal, measured with chirped probe pulses, has the same expression as that obtained with TL pulses. One can easily show the above result through a Wigner spectrogram, which provides a 2Dimensional picture of a joint time and frequency profile of a pulse. As example, in the figure 3.14, taken from *D. Polli et al.* [25], it's possible to see

that different frequency components of the pulse occur at different time. It is important to note that, while the temporal intensity profile of the chirped pulse is dramatically broadened, any horizontal cut of the Wigner Spectrogram at a given frequency preserves the duration of the TL pulse. It can be demonstrated that this is rigorously true for a pulse with a quadratic spectral phase [18].
So each slice is simply a rigid temporal translation of a TL pulse, as shown in Fig. 3.14 (f). In the presence of a significant higher-order dispersion (cubic etc.), the spectral slice is not a simple sheared replica of the TL pulse, but in general the distortions are limited. In conclusion, even in the presence of a strong frequency-chirped probe pulse one can count on the same temporal resolution provided by an equivalent nearly TL pulse with the same bandwidth.

3.3 Data Acquisition

Since probe pulses are broadband, instead of using a photodiode with a lock-in amplifier and changing the detected wavelength using different interferential filters, it is preferable to use an Optical Multichannel Analyzer (OMA)(Princeton Instruments, Acton SpectraPro SP-2150); so, after hitting the sample, the probe beam only is sent in an OMA. The OMA contains several gratings that disperse different frequency ranges on a linear CCD. Differential transmission spectrum, which is modulated at half of the laser repetition rate, is thus measured for each wavelength. Resolution is given by the CCD pixels number, the grating type and their distance, and it is typically less than $1nm$. The chosen OMA model is provided with a 512 pixel CCD and two gratings with different spacing, one grating is suitable for visible light, the other for near UV. The range that can be displayed is however smaller ($\approx 250nm$) than the actual spectrum yielded by the crystal, so the range must be chosen in accordance to the transition to be seen. The

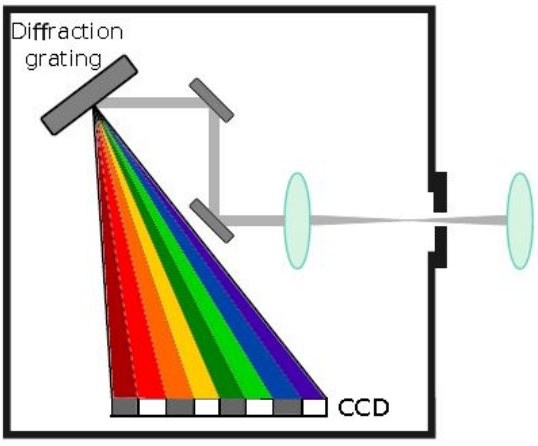

FIGURE 3.15: Optical Multichannel Analyzer on top view

control software for the experiment is written in LabVIEW. The main components to be connected to the computer are the pump-probe delay stage, the motorized rotation stage, the OMA and two linear Zaber stages. In a single pump probe experiment the OMA records spectra of probe pulses when pump is on and off, for selected delays of the stage. The motorized rotation stage position can be set with a manual controller, to select the frequency interval of probe pulses.

3.4 Experimental setup complete design

In this section we can appreciate the complete setup, including both the pump and the probe generation. It is helpful to notice in fig 3.16, how the pump and the probe pulses need to be focused on the sample after being generated. They should overlap temporally and spatially on the sample. The lens used to focus the two beam are then different: for the pump beam the convergent lens has focal of $250mm$, instead the one for the probe has $f = 200mm$. After passing through the sample the pump beam is blocked by an iris, which permits to transmit only the probe pulses at the spectrometer. The pump is chopped in order to obtain the differential transmission signal at the output. The optical chopper works at $1kHz$ frequency.

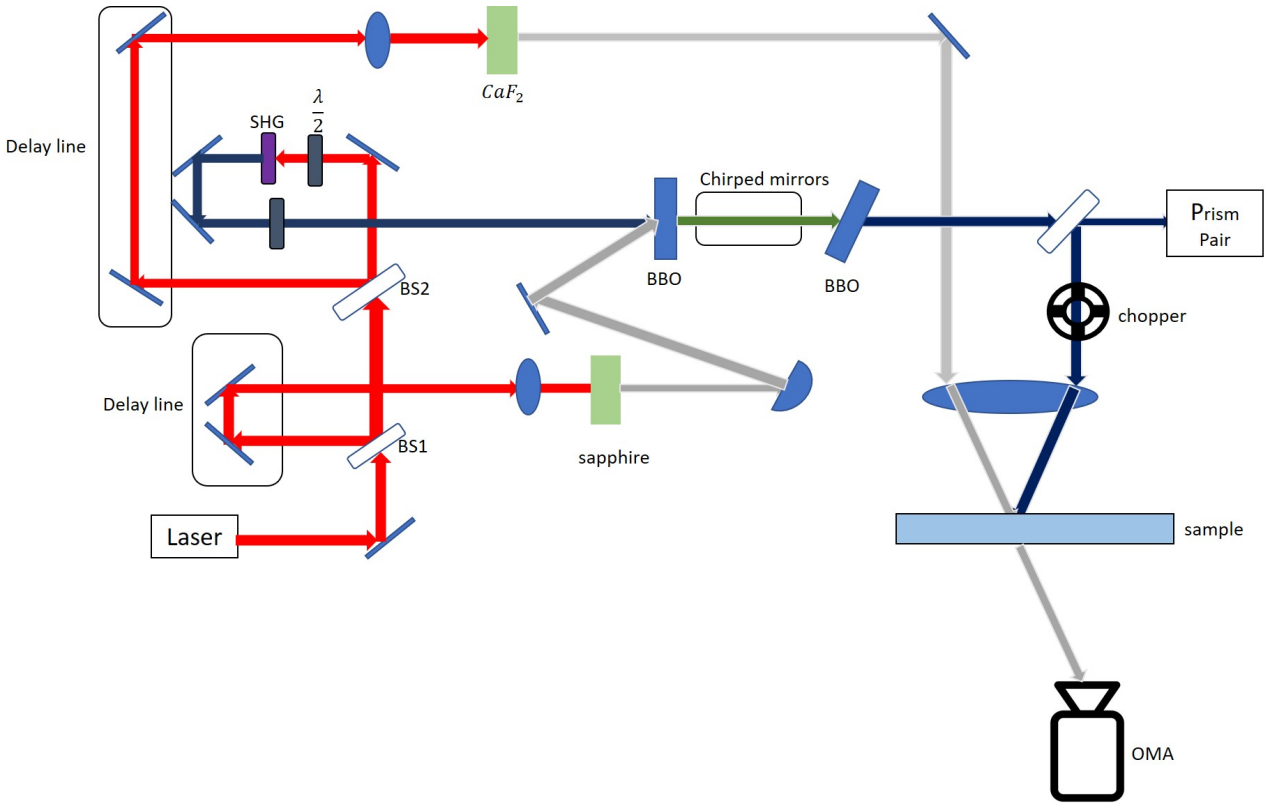

FIGURE 3.16: Complete experimental setup. BS: Beam Splitter, OMA: Optical Multichannel Analyzer, BBO: Barium Borate crystal.

3.5 Methods of Analysis

The analysis is performed using many computational tools. The use of the MatLab software is fundamental to achieve spectra, dynamics and 2D maps (joint time and probe wavelength maps).

A guided user interface (GUI), described and shown in the figure 3.17, is an helpful

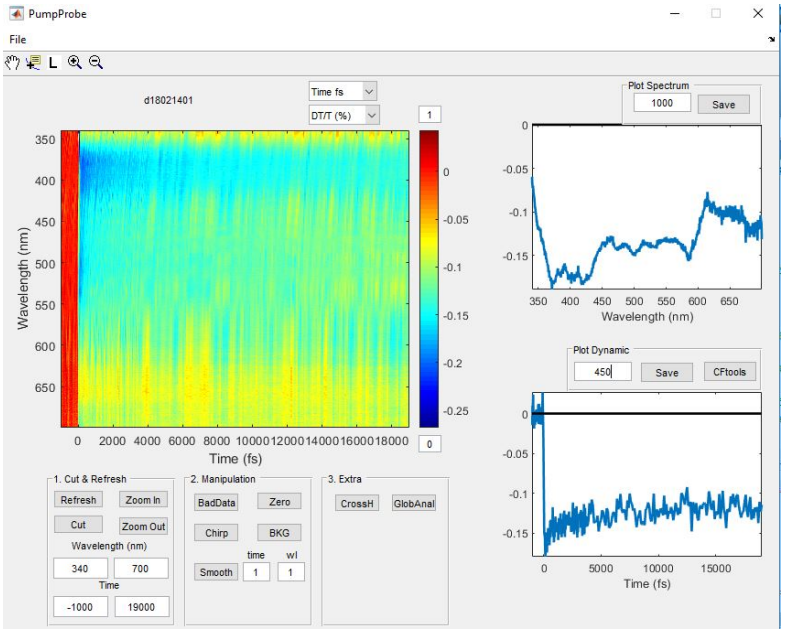

FIGURE 3.17: MatLab software used to obtain in a more compact way all the data arriving from the spectrometer

tool to analyze data coming from the OMA. Furthermore, it's possible to subtract the background and to remove the strong chirp induced by the white light generation. This is possible, as has been explained in the previous chapter, without loosing relevant temporal resolution. It is also possible to smooth the data, averaging between several adjacent time points of the spectrometer, in order to get the overall noise lowered. The other two graphs on the right side allow to obtain the differential transmission spectra for fixed time delays and dynamics for fixed probe wavelengths.

Other MatLab codes are useful to make individual fits of single probe wavelength as function of time. Starting from a known exponential function (could be mono-, bi- or tri- exponential), by several iterations is possible to get the constants which identify the lifetime of different excited states of the molecules after the pump excitation.

Another important computational tool is Glotaran. Glotaran is a free software program developed for global and target analysis of time-resolved spectroscopy and microscopy data [26]. After creating a data set, with the data taken from the OMA in the laboratory, it performs iterative analysis having as parameters the lifetime constants or alternatively the transition rate, and having explained what kind of exponential decay the process

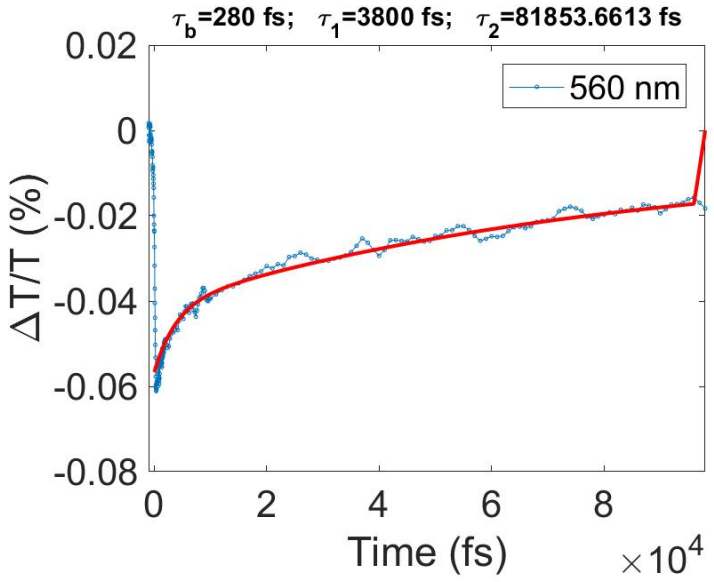

FIGURE 3.18: Individual fit of a bi-exponential decay with probe wavelength of 560 nm

occurs, the dispersion factors induced by the chirp and the impulse response function of our instrumental apparatus. It's possible to choose the maximum number of iteration before obtaining convergence. It is important to choose the correct constants in order to obtain a convergent Glotaran analysis. At the end the Glotaran analysis will give an unique lifetime constant for all the involved probe wavelengths.

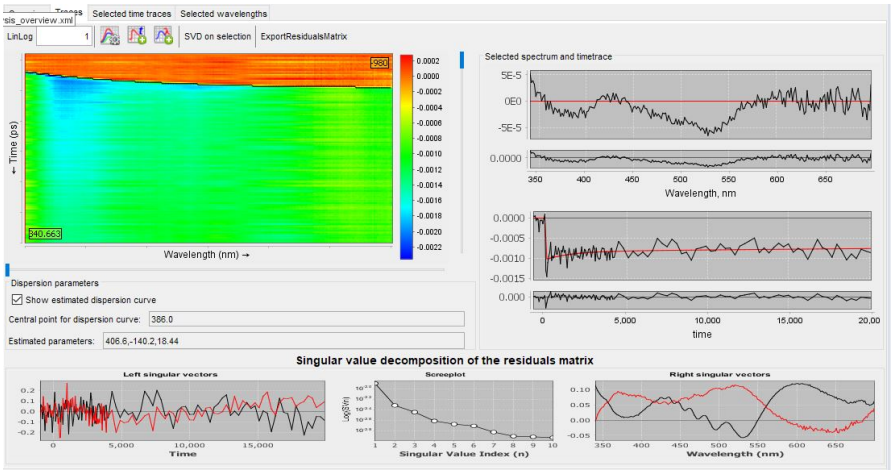

FIGURE 3.19: Example of traces in the Glotaran Analysis

Chapter 4

Experimental Results

The experimental setup discussed in the previous chapter has been used to investigate transient spectra and dynamics of photo induced biological processes. The pump is usually absorbed by these molecular compounds and then the probe could investigate the photoproduct signals which appear at different times.
My study will start from measurement on simpler compounds (aminoacids), and afterwards increase the level of complexity (proteins), because the aminoacids are used as building blocks in protein biosynthesis.

4.1 Triptophan Analysis

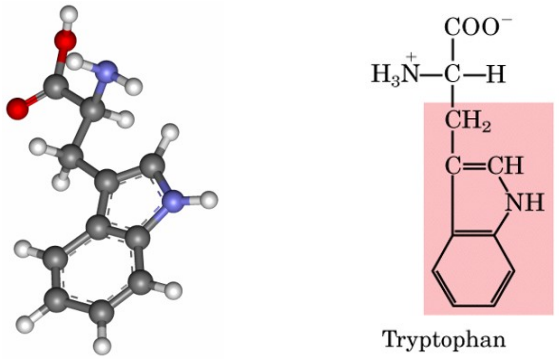

FIGURE 4.1: Molecular structure of Trp

Tryptophan (symbol Trp or W) is an α-amino acid that is used in the biosynthesis of proteins. It contains an α-amino group, an α-carboxylic acid group, and a side chain indole, making it a non-polar aromatic amino acid. It is essential in humans, meaning the body cannot synthesize it: it must be obtained from the diet. Tryptophan is also a

precursor precursors to essential compounds such as the neurotransmitters serotonin or dopamine [27].

Looking at its structure in figure 4.1, we can see how the tryptophan presents a benzenic ring, which absorbs in the UltraViolet;in fact the $\pi \rightarrow \pi^*$ transition, occurs at energies contained in the UV region of wavelengths.This aminoacid could reacts to an ultraviolet excitation as pump, creating a population difference between ground state $|0>$ and the first excited state $|1>$. Usually the aminoacid compounds are absorbing in the deep ultraviolet region, below $200nm$ in wavelength, but the Tryptophan toghether with Tyrosine, because of the presence of an aromatic ring, is resonant with transitions around $260 - 300nm$ [27]. This is easily verified by the analysis, presented in fig (4.2), of the tryptophan absorption spectrum which reveals a huge peak around 270 nm. This wavelength region is optimally reachable by ultra short pulses generated using our experimental setup configuration, by doubling in frequency the NOPA output pulses.

The experiment intent is the possibility to pump in the UV and then subsequently investigate the photo-induced absorption in the entire visible and UV range, by illuminating the sample with a broadband probe after a certain delay τ. At different delay, different signals should be obtained, and this allows us to retrieve the dynamic evolution of the aminoacid after being excited by the pump.

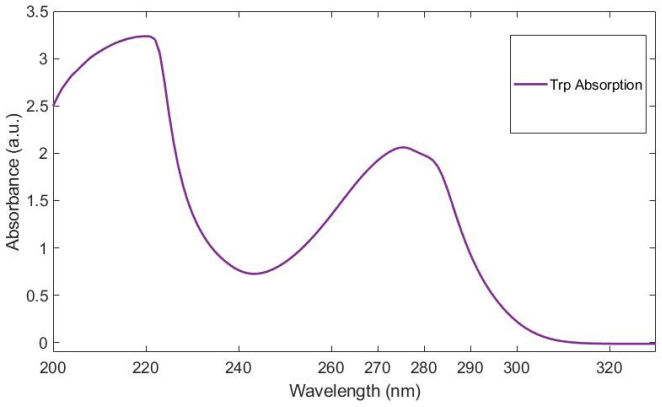

FIGURE 4.2: Absorption spectrum of Tryptophan (W) in a Phosphate Buffered Saline (PBS) solvent

Previous experimental works

Tryptophan dynamics and transient spectra have been studied in recent years. It has been discovered that Tryptophan (Trp) is the brightest fluorophore among the natural aminoacids and its photophysics depends sensitively on its molecular environment [28]. Samples of Tryptophan dissolved in water with pH 7.4, are excited by 266 nm pump pulses, and transient absorption is probed, in magic angle conditions, by a $290700nm$

white light supercontinuum generated in CaF_2 crystal [28]. When the Tryptophan is dissolved in water, its energy level representation, expressed in the scheme in figure 4.3 , showed how the excited Trp reacts after the collision of a pump beam which populates the first excited state. The excited state decays to a new state with different molecular conformation, which is called primary photo-product because is caused by a photo induced excitation of the molecule. Thus the S_1, first excited state, quenching populates a new triplet state called the photoproduct. This process is still a debated pH-dependent mechanism which may involve an excited-state proton or electron transfer. The quenching of the excited state occurs simultaneously with a rise of two absorption bands centred respectively at 360 and 425 nm. They can be seen as the photoproduct signatures[29]. The measurements are taken up to some ns delay, in order to get both the fast and the slow transient signals. The fast process is the solvent relaxation of excited Tryptophan which causes the formation of protonated zwitterionic form of Trp known as photoproduct. The constant of the solvent relaxation should be of the order of $1ps$. then more time constants are found for longer delays (around $500ps$ and $3ns$), which are in very good agreement with the time constants that characterize the multi-exponential decay of the Trp fluorescence [30]. This should convince us that the two absorption bands derived from the photoproduct formation (P_1 and P_2), are present for very long time. Measuring for longer delays between pump and probe beams, up to $6ns$, reveals also

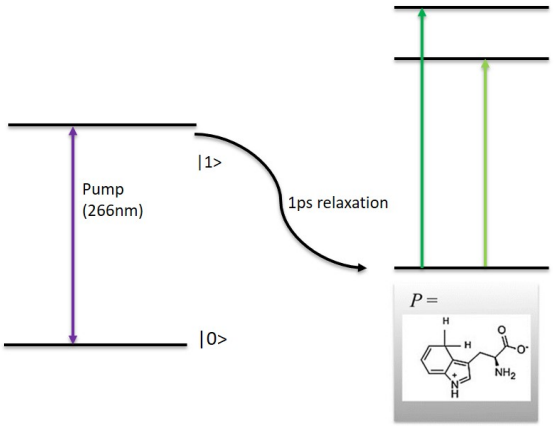

FIGURE 4.3: Energy level sketch of the Tryptophan investigated with Uv pump-probe experiment

the presence of two quasi isosbestic points observed at $475nm$ and around $350nm$. This points represent the simultaneous presence of two different compounds in equilibrium with each other, the photoproduct and the Tryptophan radical, that still could be neutral ($T^{\cdot}$or a cation ($TH^{\cdot+}$). From the spectra 4.4, the graph on the right, it is noticeable also how the residual signal by the solvent becomes relevant at longer probe wavelengths.

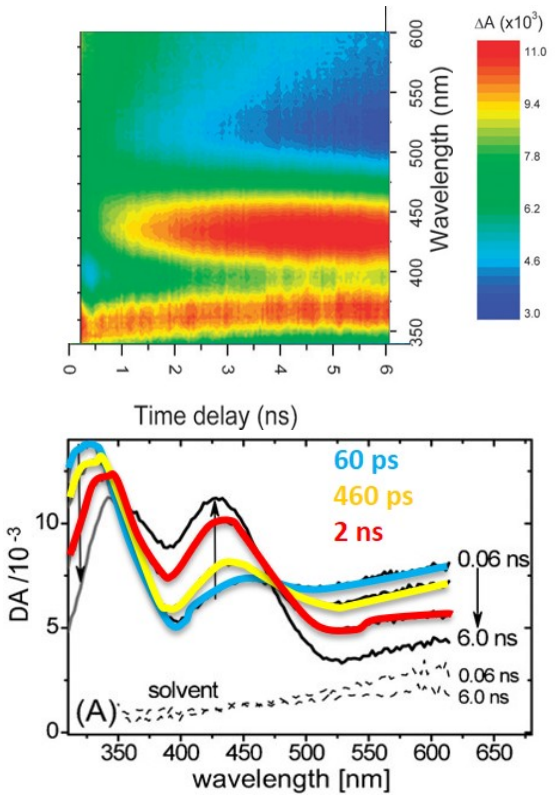

FIGURE 4.4: Trp differential absorption as function of the delay between pump and probe[28].

Tryptophan experimental Data

We measured Tryptophan with our ultrafast pump-probe spectrometer in the ultra-violet wavelength region. We will measure the differential transmission instead of differential absorption of the previous works.
With our experimental setup, described in the previous chapter, we are able to excite this molecule with a pump beam of $270nm$ $(4.6eV)$. The probe is made by a white light continuum generation through a CaF_2 crystal. Moreover the Tryptophan is dissolved in PBS (Phosphate Buffered Saline) which stabilizes pH at 7.4 and it is present with a concentration of $0.02mmol/ml$. The solution flows into a cuvette with length of 200 μm in the propagation axis of light, with a fluence of approximately $5\mu J/cm^2$.

Visible probe light

To begin with, we start applying a visible probe, using CaF_2 obtaining an approximately noise free range of white light from $350nm$ up to $650nm$. From the figures 4.5 and 4.6 it could be seen an increasing negative signal during the first picoseconds around $350nm$

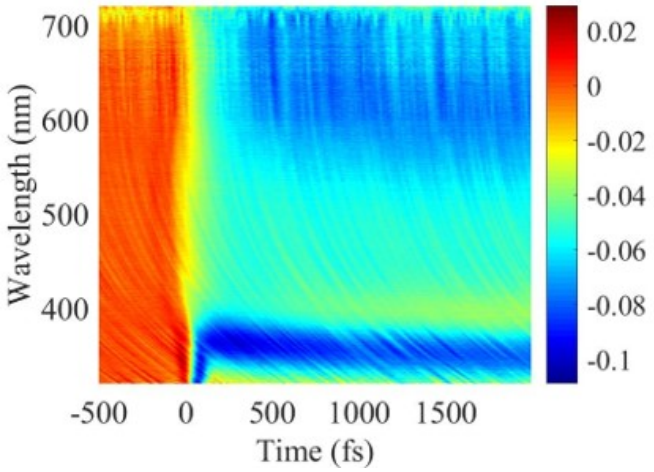

FIGURE 4.5: Tryptophan differential transmission map, pumping at 270

while almost nothing is noticed at frequencies around $450 - 500nm$. This could be explained noticing that the absorption band P_1 occurs more rapidly with respect to the other photo-product absorption band P_2.

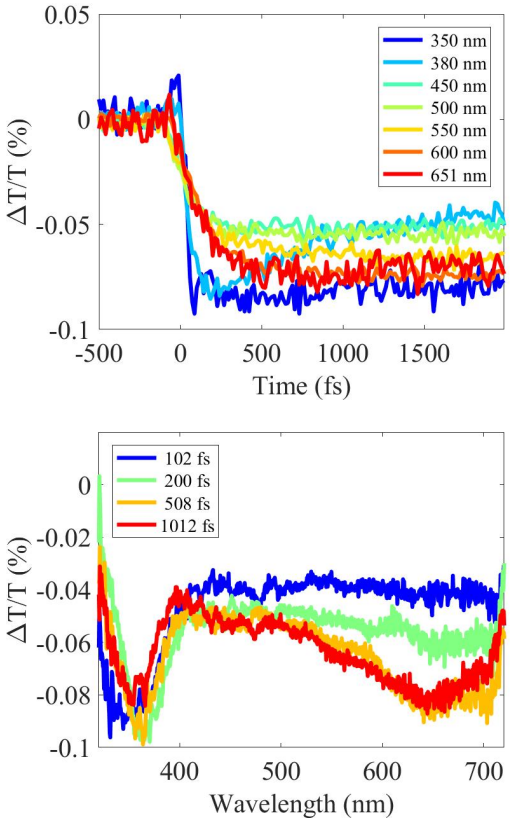

FIGURE 4.6: On top time dynamic comparison for different wavelength. On bottom transient spectra for different time delay.

It is present in the dynamics also a build up around $600nm$, which refers to a band formation around that wavelength.

It is helpful to analyze the individual wavelength fits in order to collect information on the nature of the Trp pump-probe dynamics. It is evident from the graphs that the dynamics follow a bi-exponential decay, with a short constant in the first picosecond and longer one. These two constants are in a quite good agreement with the previous analysis made by *Leonard et al.* [28]. The function used to fit the data is the following.

$$f(t) \sim [A_1 * e^{-\frac{(t-t_0)}{\tau_1}} + A_2 * e^{-\frac{t-t_0}{\tau_2}}] * He(t-t_0)$$

where t_0 is when the signal start, which is different for each wavelength because of frequency chirp, and τ is the decaying constant. One could see also how higher energies, so lower wavelengths, have slightly shorter decays which explains the faster comparison of P_1 with respect to P_2 band.

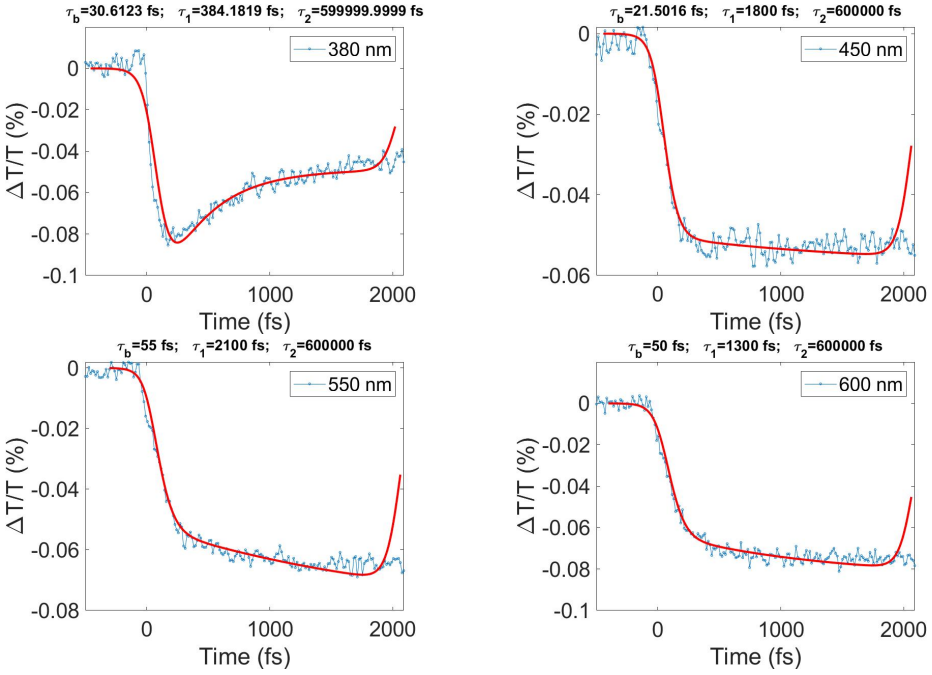

FIGURE 4.7: Individual exponential fits of different probe wavelengths

Ultra violet probe light

Once got the results on the excited state absorption in the visible it is helpful to spread our investigation in the ultra violet region. In order to get this we use the second configuration for the broadband probe generation, making an up-conversion in frequency (second harmonic generation), before the white light generation (through $\chi^{(3)}$, the third order susceptibility). With our configuration we can enlarge our frequency range from 300 up to $360nm$, with a reasonable amount of noise fluctuations.

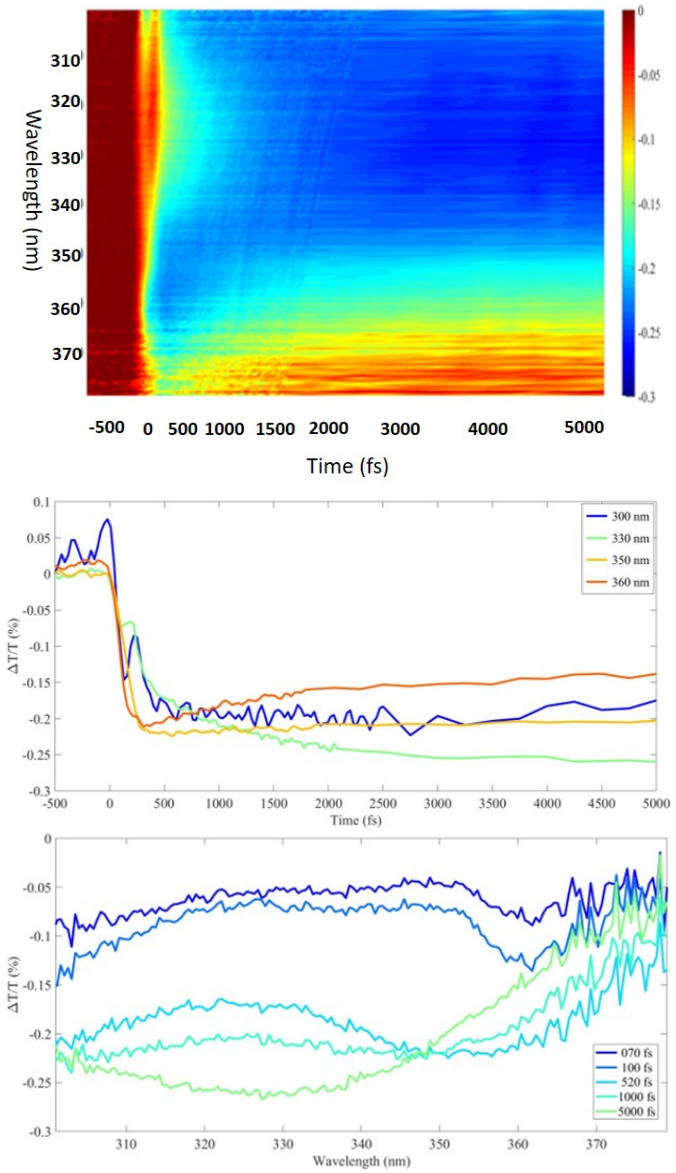

FIGURE 4.8: Pump probe experimental data using an ultra violet broadband beam as a probe

From the analyzed data of figure 4.8 we can start making some more complex considerations. Firstly, from the $2D$ map we can assume that after $350nm$ the absorption starts to decrease at least until $360nm$. Looking to the spectra in the same figure (on bottom), we can clearly see the appearance of an isosbestic point after a couple of ps. It is important to notice also that for the first $200/300fs$, there is no huge absorption which starts growing after the ps solvent caused relaxation as predicted. The presence of the isosbestic point in the differential transmission transient spectra should be a consistent proof of the faster behaviour of P_1 between the two bands derived by the photo-product formation. Looking to the individual wavelengths fit, in figure (4.9) it is possible to retrieve the biexponential decay, similarly to what we did investigating with a visible probe. Moreover we can notice how there is a band formation after one picosecond around $330nm$.

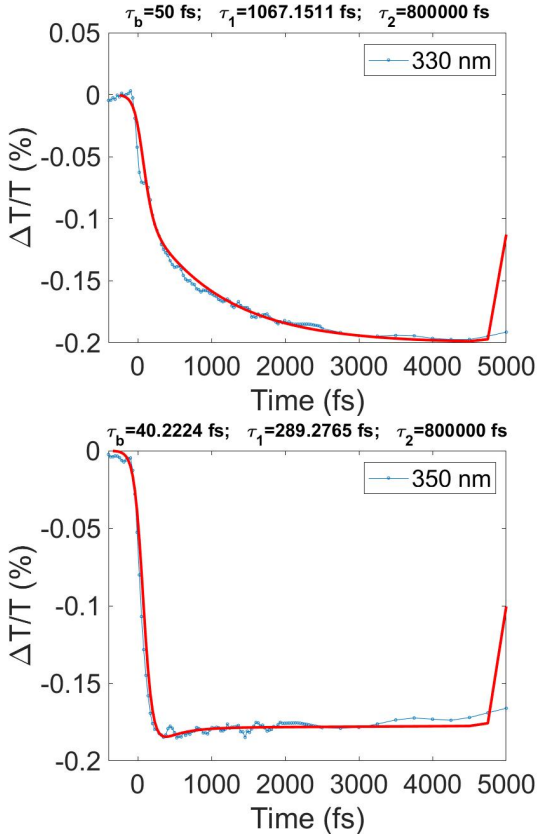

FIGURE 4.9: Individual fit for probe wavelengths of 330 and 350 nm

The presence of a second very long time constant in the bi-exponential decays suggested us to start investigating longer delays (up to $1.5ns$) in order to better understand the presence of the two isosbestic point and the corresponding absorption bands.

Performing longer measurements

We change the experimental setup to reach longer delays with the pump-probe spectroscopic measurements. It is possible to neglect the compression system because now we are not anymore limited by strict time resolution requirements. The pump is now obtained via third harmonic generation directly from the fundamental beam coming from the Titanium sapphire laser source. In figure 4.10 it's presented the setup configuration that we used to obtain $266nm$ pump pulse from the fundamental source $800nm$.

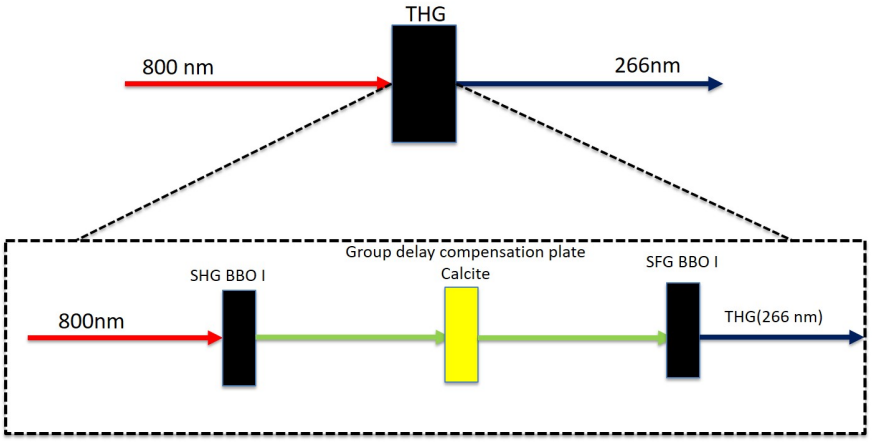

FIGURE 4.10: Block scheme of the Third harmonic generation setup from the fundamental laser source

The most important blocks are two BBO which are used respectively for the second harmonic generation and the sum frequency generation to obtain at the output $266nm$ pulses. It's very important the presence of a compensation plate between the two, in our case is Calcite, because it adjusts the group delay difference created by the different group velocity of the fundamental and the second harmonic after the first BBO crystal, in order to maximize the efficiency of the SFG. The probe pulse is still generated via white light continuum by the mean of a CaF_2 crystal plate, with no need of compression as explained in the previous chapter.
Trying to make a better comparison with the paper results I will present a $2D$ map as function of differential absorption instead of transmission, actually obtained change the method of calculation.
As we could see from 4.11, the map is pretty similar to figure 4.4 reflecting the huge and long lasting absorption peak around $350nm$.

Looking to various spectra and dynamics is interesting to see how the Isosbestic point is pretty stable at $450nm$. We can evince that also looking at the dynamics plot, where the $450nm$ decay seems to be pretty flat after few picoseconds. The signal that we

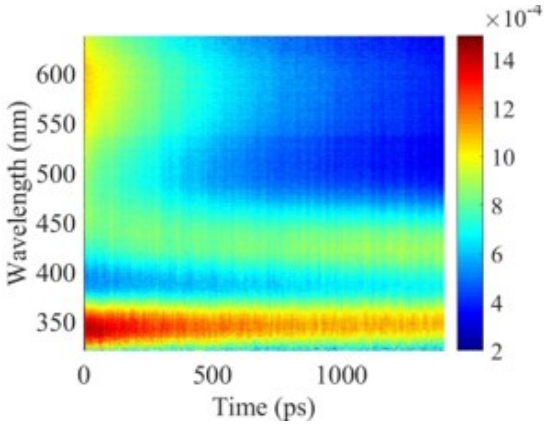

FIGURE 4.11: Experimental Data of differential absorption obtained pumping at $266nm$

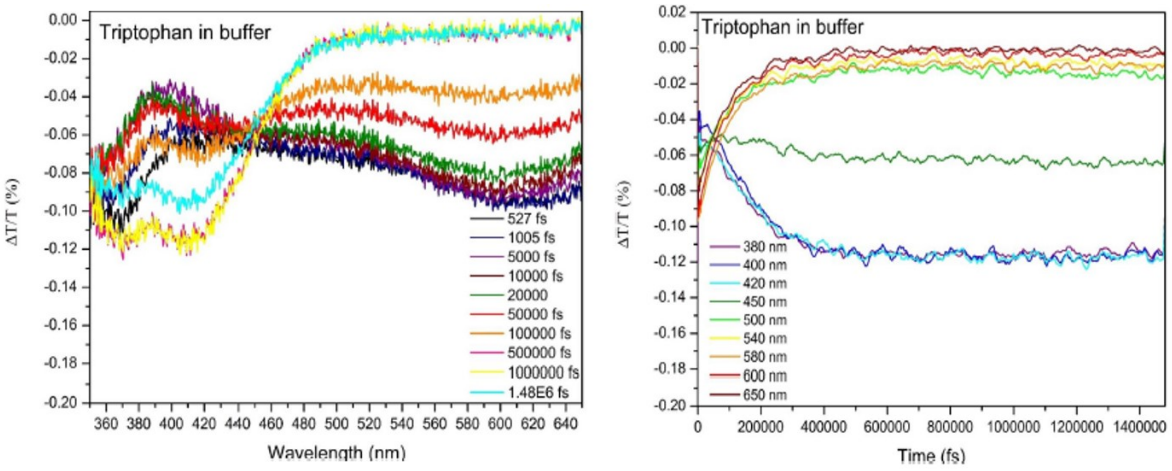

FIGURE 4.12: Spectra and Dynamics for different delays

can appreciate there is the intersystem crossing between a singlet and a triplet state. This effect is radiationless and involves a transition between two electronic states with different spin multiplicity.[31] Indeed it is possible to assume that the photoproduct of the Trp might be a precursor for the phosphorescent triplet state ${}^{T}TrpH$, metastable and with a neutral indole. However more work should be done in order to determine the quantum efficiency of this process and the kinetics associated to the P decays.

Furthermore, it could be interesting to study faster transient signals of the Trp, trying to understand which are the mechanisms which could appear before the solvent relaxation and its consequences: as an example could be helpful to study the excited state absorption of Trp before the S_1 quenching.

4.2 Preliminary test on Azurin

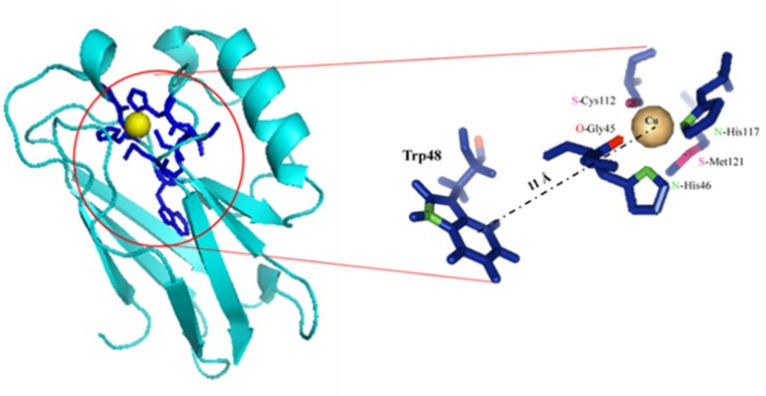

FIGURE 4.13: Molecular 3D structure of the Azurin protein with particular mention to the Trp-Cu bond.

Moving to further complexity we would investigate the behaviour of Tryptophan inside more complex systems, like proteins. As protein we investigated Azurin, which presents a Tryptophan radical very close to a metal. Azurin is a bacterial blue copper protein found in Pseudomonas, Bordetella, or Alcaligenes bacteria, which undergoes oxidation-reduction between Cu(I) and Cu(II) [32]. The ability of transition metals to exist in more than one stable oxidation state makes them suitable catalysts for biological processes that require transfer of electrons [33]. Indeed our study will be partly focused on the excitation of Tryptophan absorption band in the azurin in order to see which mechanism is associated with the energy transfer between the Trp itself and the Copper present in this protein. Looking at the absorption spectrum in figure 4.14 it can be seen

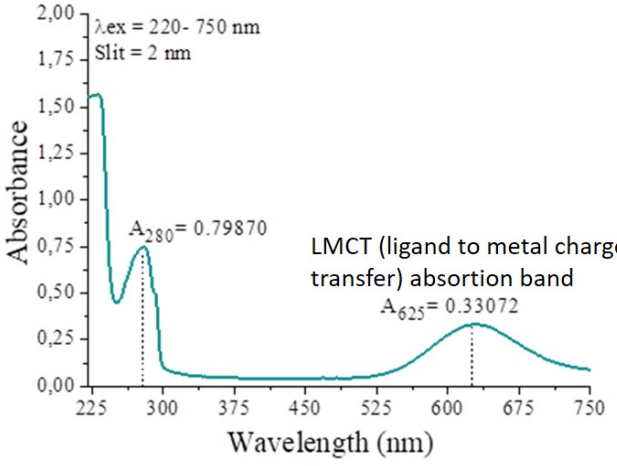

FIGURE 4.14: Azurin absorption spectrum

that the Azurin presents another absorption band, associated to the ligand to metal

charge transfer which lies around the $600nm$ region. Femtosecond pump probe spectroscopy was already applied on the LMCT band of this protein, particularly because it gives information on the excited state nuclear dynamics [34]. From the paper *Cimei et al.* [34] we expect oscillations mono-exponentially damped with a constant of $270fs$.
Moreover figure 4.14 shows that the tryptophan absorption is red shifted, because of that we will pump at $290nm$, which is still obtainable with our setup (providing pump pulses going from 260 up to 300 nm frequency range).
Some experimental data are presented below, pumping in the ultra violet range ($290nm$), and testing with both visible and Uv probe beams. We are still investigating which process is happening during the electron transfer. It's important to state that when one electron transfers from the Tryptophan benzenic ring t0 the Copper site, two possible effects could theoretically appear: Energy transfer or charge transfer.
a) In the first case energy transfer should be witnessed by the increase of LMCT absorption band in the visible range

$$h\nu + Trp \rightarrow Trp^{*} \rightarrow ET + Cu^{++}$$
$$\text{ET+Cu}^{++} \rightarrow Cu^{++} + LMCT^{+}$$

b) In the latter case charge transfer should be witnessed by a bleaching of the LMTC absorption band and should be concomitant with the generation of a Trp radical cation ($Trp^{\bullet+}$):

$$h\nu + Trp \rightarrow Trp^{\bullet+} + e^{-}$$
$$e^{-} + Cu^{++} \rightarrow Cu^{+} + LMCT^{-} \qquad [35]$$

The data are presented below with the 2D maps of differential transmission 4.16, function of delay and probe wavelength, obtained adapting the setup to obtain both visible and UV white probe. The pump remains unchanged (290 nm) and the pump probe polarization difference is at the magic angle (54). The azurin concentration is full-filled to obtain absorption of 0.9 OD at $290nm$ and the measurements are performed using a $200\mu m$ cuvette. The probe energy flowing through the sample is roughly $30nJ$ in both cases. From these two maps it's possible to evince that a strong negative signal (strong photoinduced absorption) is present between 350 and 450 nm lasting for even long delays.
The dynamics seem to follow a bi-exponential decay with a very fast first constant (of the order of 1500fs) and another very long constant, that is beyond the limiting delay of our experimental configuration.
We discuss the Azurin data mostly in comparison with the Tryptophan ones. Indeed we excite with an UV pump the Trp inside the Azurin protein (pumping at $290nm$). Trp has

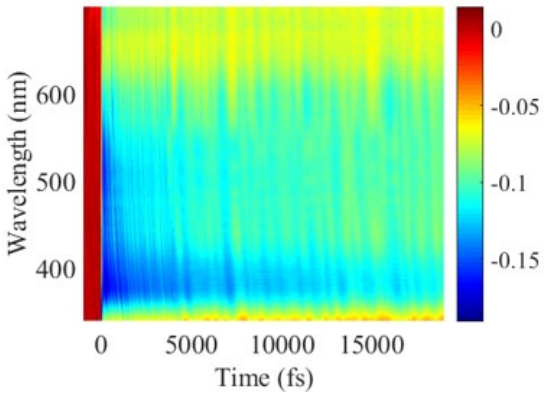

(a)

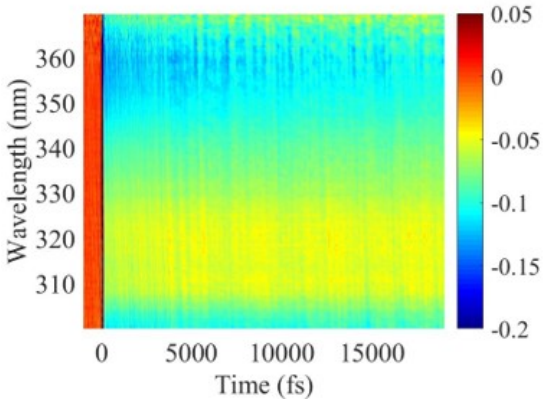

(b)

FIGURE 4.15: Experimental data of differential transmission of azurrin pumping at 290nm a) using visible and b) Uv white light probe beam

been already studied linked to other metal: For instance Tryptophan-to-HemeElectron Transfer in Myoglobins was revealed by UV 2D Spectroscopy [7], which discovers an energy transfer between Trp and iron (Fe) present in myoglobins. Moreover the metallo proteins present very particular and unique features. I will present below some figures in which I compared spectra and dynamics of Trp (was pumped at 270nm) and Azu (pumped at 290nm). It's important to say that the dynamics were normalized, although the spectra are not.

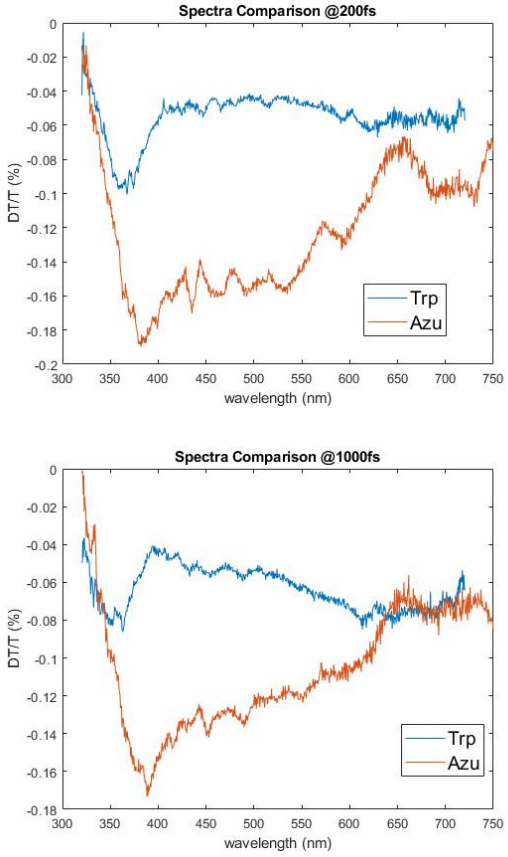

FIGURE 4.16: Spectra comparisons of Tryptophan (blue curves) and Azurrin(red curves)

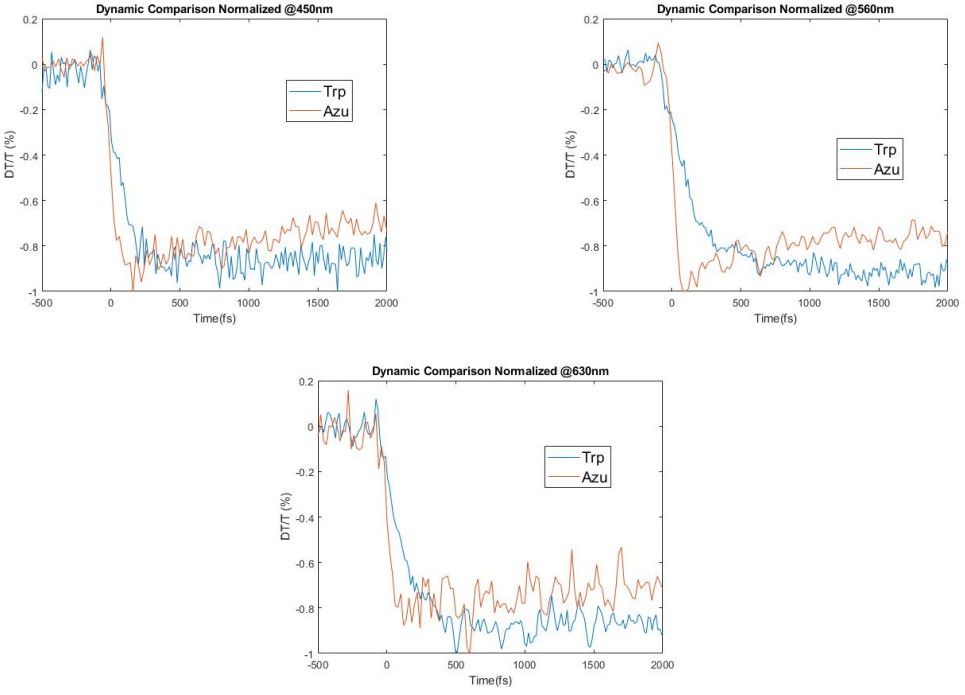

FIGURE 4.17: Dynamic comparisons of Tryptophan (blue curves) and Azurin (red curves)

We also perform a global fit analysis of every wavelength made with Glotaran software tool as shown in figure 4.18. We can see how the bi-exponential decay is retreived with two lifetime constants ($\tau_1 = 1.6ps$ and $\tau_2 = 220ps$). From this analysis it is possible even to recognize the impulse response function of our setup which is modeled by a coherent artefact (Cohspec node in the programme), which presents two constants respectively at 17 and 26 fs. To perform further investigations involving longer time constants, could be

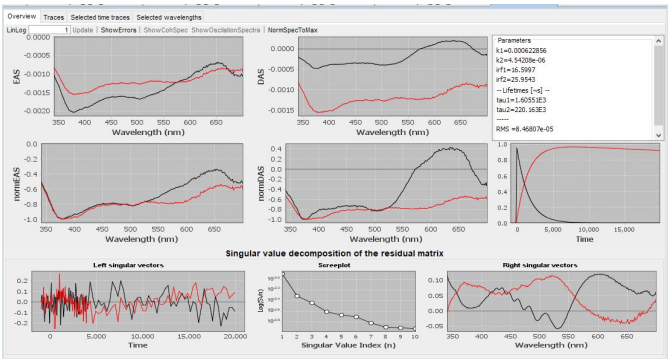

FIGURE 4.18: Lifetime analysis with Glotaran using visible probe Azurrin analysis

appropriate analyzing the azurin behaviour on longer delays, as we did for Tryptophan, in order to understand better the slower behaviour of tryptophan inside this protein.

Pumping the LMCT band

Other measurements were performed aiming at verifying the previous experimental results by *Cerullo et al.* [35]. In this case we want to test the system after the excitation of the ligand to metal charge transfer absorption band; in order to do that we pump the system with an ultra short pulse at $630nm$. Now, we are not limited from the strong requirements of UV frequency range, because our pump is in the visible region of frequencies. So we use the output of the non-collinear OPA, after the proper compression made by chirped mirrors, as the pump beam. Looking at the visible dynamics for different wavelengths, in figure 4.19 we could notice how the expected oscillations take place. This measurements were taken with the same conditions as the one pumped at $290nm$, however the probe energy is higher ($E = 90nJ$). It is possible to say that in the dynamics are present oscillations damped after few hundreds of femtosecond as was expected from the theory. We study these oscillations making a fit with an exponential function of the form

$$f(t) = Aexp(-\frac{t}{\tau})$$

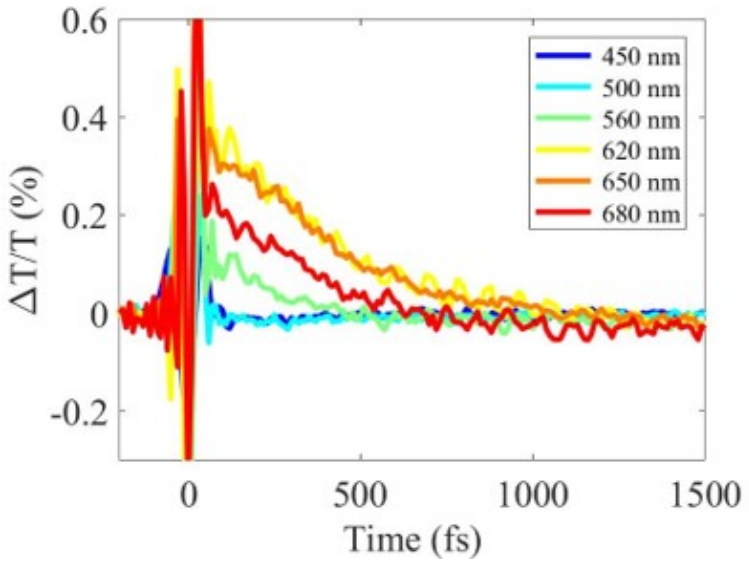

FIGURE 4.19: Dynamics of the Azurrin sample after the excitation at $630nm$

where the value are taken from the previous experiments (amplitude $A = 0.4\%$ and $\tau = 270fs$)[35]. We start extrapolating the dynamic of a single wavelength ($620nm$), and after having applied the fit with the previously explained function, we are able to calculate the residuals, which consist in the frequency oscillations, as can be seen from figure 4.20 Through a discrete Fourier transform we are able to retrieve complex number

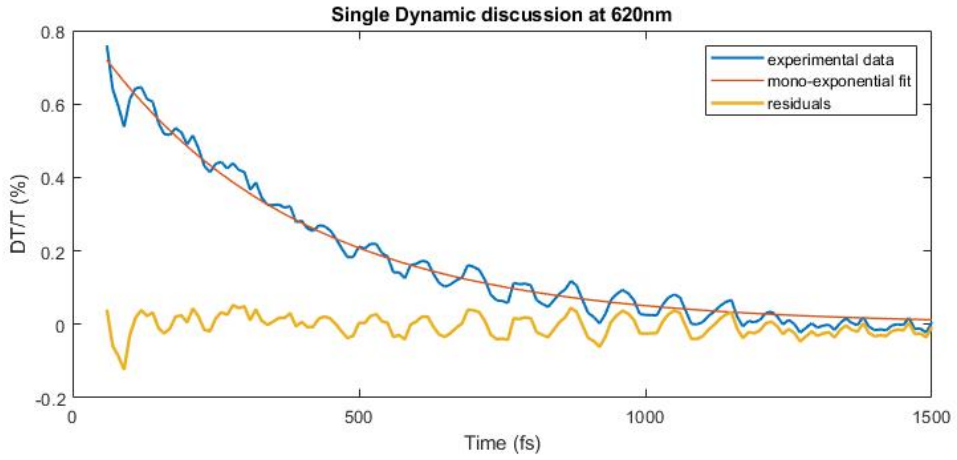

FIGURE 4.20: Single wavelength fit at 620 nm, fitted in order to retrieve the oscillating residuals.

associated to the frequency analogous of the oscillations in time. Then by applying the square modulus, multiplying for the complex conjugate each complex quantity, it is possible to meet the frequency of the oscillations, which results in $13THz$, around $400cm^{-1}$.

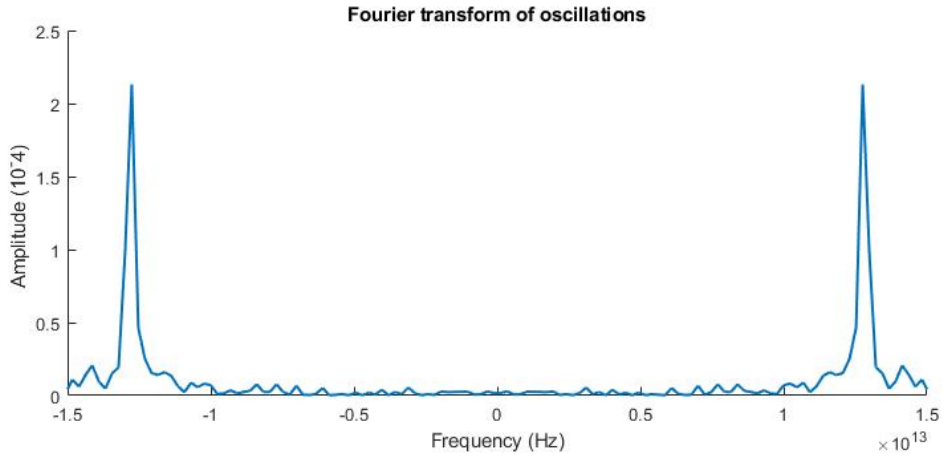

FIGURE 4.21: Amplitude obtained through the discrete fourier transform calculations.

Chapter 5

Conclusion

In this thesis we developed and characterized a pump-probe spectroscopy setup in the ultraviolet range, aimed at the study of structural conformations of relevant biomolecules and at the analysis of ultra fast processes in which biomolecules are involved. The first requirement is to ensure high temporal resolution, that is very difficult to obtain with a non collinear Optical parametric amplifier in the UV frequency range because of many issues. The crystals are highly dispersive in the ultra violet, because the impinging photon have very high energy, the phase control is more difficult than for a visible output of an OPA and the two-photon absorption could hamper the success of this setup development. To avoid this issues the output of the NOPA is doubled in frequency through second harmonic generation in a BBO crystal.Another compression, usually with prisms, is needed to remove the pathway dispersion. At the output we will obtain broadband pulses ($260 - 300nm$), with energy around $40 - 50nJ$ and duration of 16 fs.
These pump pulses are good to analyze aromatic aminoacids and proteins which are very resonant in this frequency region because of the presence of a benzenic ring.
The setup allows for the generation of a white light continuum either in the visible or in the ultraviolet range, focusing the laser fundamental ($800nm$) or second harmonic ($400nm$) pulses in a sapphire or calcium fluoride plate. Hence the sample under study can be probed in the whole $260 - 700$ nm range.
We showed also how was possible to exploit the relaxation constant of Tryptophan and the intra-molecular transfer in protein.
This setup could be used to analyze ultra fast processes appearing in the biomolecules, like the very fast Tryptophan absorption band, thanks to the very high resolution and precision that is impossible to achieve using electronic systems. This is an helpful tool to investigate the natural phenomena which appear instantaneously, like the aminoacid mechanisms of photo-protection.

Moreover, recently, understanding the mechanism of electron transduction through biological macromolecule has become of fundamental importance not only in increasing our knowledge of the electron transfer process, ubiquitous in biology, but also in the development of novel, improved bioelectronic devices.[36] This leads to develop innovative hybrid nano-bio-devices with potential applications in the fields of biosensing, bioelectronics, conversion and storage of energy, etc. [37] Indeed, metallo-proteins, appropriately anchored to conductive substrates, can constitute the core of innovative nano-devices with the capability to perform multiple functions.

Bibliography

[1] K. P. Lawrence, A.R. Young, and P. F. Long. Mycosporine-like amino acids for skin photoprotection. 2017.

[2] Cristian Manzoni and Giulio Cerullo. Design criteria for ultrafast optical parametric amplifiers. *Journal of Optics*, 18:1–33, August 2016.

[3] G. Grancini, M. Maiuri, D. Fazzi, A. Petrozza, D. Brida, G. Cerullo, and G. Lanzani. Hot exciton dissociation in polymer solar cells. 2012.

[4] D. Polli, Alto P, Weingart O, Spillane KM, Manzoni C, Brida D, Tomasello G, Orlandi G, Kukura P, Mathies RA, Garavelli M, and Cerullo G. Conical intersection dynamics of the primary photoisomerization event in vision. *Nature Communications*, 2013.

[5] D. Brida, A. Tomadin, C. Manzoni, Y. J. Kim, A. Lombardo, S. Milana, R. R. Nair, K. Novoselov, G. Cerullo, and M. Polini. Ultrafast collinear scattering and carrier multiplication in graphene. 2012.

[6] V.R. Young. Adult amino acid requirements: the case for a major revision in current recommendations. 1994.

[7] Cristina Consani, Gerald Aubck, Frank van Mourik, and Majed Chergui. Ultrafast tryptophan-to-heme electron transfer in myoglobins revealed by uv 2d spectroscopy. 2015.

[8] A.H. Zewail. Femtochemistry: Atomic-scale dynamics of the chemical bond. *Chemical Physics*, 2000.

[9] D. A. Kleinman, A. Ashkin, and G. D. Boyd. Second-harmonic generation of light by focused laser beams. *Physical Review*, 145(1):338–379, 1966.

[10] Jean-Claude Diels and Wolfgang Rudolph. Ultrashort laser pulse phenomena. *Academic press*, pages 623–624, 2006.

[11] M. Houe and P. D. Townsend. An introduction to methods of periodic poling for second-harmonic generation. *Journal of Physics D: Applied Physics*, 28:1–18, August 1995.

[12] R. Huber, H. Satzger, W. Zinth, and J. Wachtveitl. Noncollinear optical parametric amplifiers with output 622 parameters improved by the application of a white light continuum generated in caf2. *Optical Communications*, pages 443–448, 2001.

[13] Rocio Borrego-Varillas, Lucia Ganzer, Giulio Cerullo, and Christian Manzoni. Ultraviolet transient absorption spectrometer with sub-20-fs time resolution.

[14] Francesco Morichetti, Andrea Melloni, Jaroslav Cap, Jiri Petracek, Peter Bienstman, Gino Priem, Bjorn Maes, Michele Lauritano, and Gaetano Bellanca. Self-phase modulation in slow-wave structures: A comparative numerical analysis. *Optical and Quantum Electronics*, 38:761–780, 2006.

[15] Andrew M.Weiner. Ultrafast optics. 2009.

[16] Larry Luer Giulio Cerullo, Cristian Manzoni and Dario Polli. Timeresolved methods in biophysics. 4. broadband pumpprobe spectroscopy system with sub-20 fs temporal resolution for the study of energy transfer processes in photosynthesis. *Photochemistry Photobiology Science*, 6:135–144, 2007.

[17] D. Polli, D. Brida, S. Mukamel, G. Lanzani, and G. Cerullo. Effective temporal resolution in pump-probe spectroscopy with strongly chirped pulses. *Optical Physics*, 82, 2010.

[18] S. De Silvestri, C. Manzoni, R. Borrego-Varillas, A. Oriana, and G. Cerullo. Tunable few-optical cycle pulses and advanced ultrafast spectroscopic techniques. *Il Nuovo Cimento*, 2018.

[19] C. Manzoni Y.J. Kim A. Lombardo S. Milana R.R. Nair K.S. Novoselov A.C. Ferrari G. Cerullo D. Brida, A. Tomadin and M. Polini2. Ultrafast collinear scattering and carrier multiplication in graphene. *Nature Communications*, 1984, 2013.

[20] Dario Polli, Piero Altoe'and Oliver Weingart, Katelyn M. Spillane, Cristian Manzoni, Daniele Brida, Gaia Tomasello andGiorgio Orlandi, Philipp Kukura, Richard A. Mathies, Marco Garavelli, and Giulio Cerullo. Conical intersection dynamics of the primary photoisomerization event in vision. *Nature Communications*, 2010.

[21] V. R. Bhardwaj, E. Simovaa, P. B. Corkum, and D. M. Rayner. Femtosecond laser-induced refractive index modification in multicomponent glasses. *journal of Applied Physics*, 2005.

[22] R R Alfano, Q X Li, T Jimbo, J T Manassah, and P P Ho. Induced spectral broadening of a weak picosecond pulse in glass produced by an intense picosecond pulse. *Optics Letters*, 11:626–628, 1986.

[23] M. Bradler, P. Baum, and E. Riedle. Femtosecond continuum generation in bulk laser host materials with sub-j pump pulses. *Applied Physics*, pages 561–5674, 2009.

[24] F. X. Kartner. Few-cycle laser pulse generation and its applications. topics in applied physics. *Springer*, 95, 2004.

[25] D. Polli, D. Brida, S. Mukamel, G. Lanzani, and G. Cerullo. Effective temporal resolution in pump-probe spectroscopy with strongly chirped pulses. *Physics Review*, 2010.

[26] Joris J. Snellenburg, Sergey Laptenok, Ralf Seger, Katharine M. Mullen, and Ivo H. M. van Stokkum. Glotaran: A java-based graphical user interface for the r package timp. 2012.

[27] A. Rondi, L. Bonacina, A. Trisorio, Haurib, and J.P. Wolf. Coherent manipulation of free amino acids fluorescence. *Chemical Physics*, pages 9317–9322, March 2012.

[28] J. Leonard, D. Sharma, B. Szafarowicz, K. Torgasin, and S. Haacke. Formation dynamics and nature of tryptophans primary photoproduct in aqueous solution. *Chemical Physics*, 2010.

[29] Divya Sharma, Jrmie Lonard, and Stefan Haacke. Ultrafast excited-state dynamics of tryptophan in water observed by transient absorption spectroscopy. *Chemical Physics Letters*, pages 99–102, 2010.

[30] A.Rondi, L. Bonacina, A. Trisorio, C. Hauri, and J. P. Wolf. Coherent manipulation of free amino acids fluorescence. *Chemical Physics*, 2012.

[31]

[32] B. Goran Karlsson, Torbjorn Pascher, Margareta Nordling, Rolf H.A. Arvidsson, and Lennart G. Lundberg. Expression of the blue copper protein azurin from pseudomonas aeruginosa in escherichia coli. 246, 1989.

[33] A R Bizzarri and S Cannistraro. Biophysics: Electron transfer in metalloproteins. 2016.

[34] Tiziana Cimei, Anna Rita Bizzarri, Giulio Cerullo, Sandro De Silvestri, and Salvatore Cannistraro. Excited state charge-transfer dynamics study of poplar plastocyanin by ultrafast pump-probe spectroscopy and molecular dynamics simulation. *Biophysical Chemistry*, 2003.

[35] G Cerullo. Study of the tryptophan excited state dynamics in copper azurin by applying ultrafast spectroscopy.

[36] H. B. Gray and J.R. Winkler. Electron flow through metalloproteins. 2010.

[37] Bonanni, Andolfi, Bizarri, and Cannistraro. Functional metalloproteins integrated with conductive substrates: Detecting single molecules and sensing individual recognition events. *Chemical Physics*, 2007.